Radiation Physics and Chemistry 130 (2017) 459–479

Contents lists available at ScienceDirect

Radiation Physics and Chemistry

journal homepage: www.elsevier.com/locate/radphyschem

An electron-impact cross section data set (10 eV–1 keV) of DNA constituents based on consistent experimental data: A requisite for Monte Carlo simulations

Marion U. Bug[a,*], Woon Yong Baek[a], Hans Rabus[a], Carmen Villagrasa[b], Sylvain Meylan[b], Anatoly B. Rosenfeld[c]

[a] Physikalisch-Technische Bundesanstalt (PTB), Bundesallee 100, 38116 Braunschweig, Germany
[b] Institut de Radioprotection et de Sûreté Nucléaire (IRSN), PRP/HOM/SDE/LDRI, B.P 17, 92262 Fontenay aux Roses, France
[c] Centre for Medical Radiation Physics (CMRP), University of Wollongong, Wollongong, New South Wales 2522, Australia

ARTICLE INFO

Keywords:
Electron cross section
DNA cross section
PTra
Geant4-DNA
Track structure simulation
Double differential cross section

ABSTRACT

This work provides the first cross section data set of DNA constituents for an impact of electrons in the energy range between about 10 eV and 1 keV on a DNA target. The data set is designed for an implementation in Monte Carlo simulations and consists of model functions, taking into account elastic scattering, ionization and excitation interactions with the DNA constituents tetrahydrofuran, trimethylphosphate, pyrimidine and purine. It was developed on the basis of experimentally determined absolute differential and total scattering cross sections in accordance with the available literature data. The data set will be available in the Geant4-DNA toolkit to allow secondary electron transport in a DNA-like medium down to the ionization threshold.

1. Introduction

Ionizing radiation can damage the DNA in biological cells, which potentially leads to subsequent carcinogenesis or cell death. As the DNA is a target structure on the order of a few nanometers in size, the stochastic spatial distribution of single interactions has to be taken into account to evaluate DNA damage. This is achieved by track structure simulations, in which the interaction history of incident and liberated particles is followed step-by-step until their energy falls below a specified threshold (given, for example, by the limitations of underlying physical data or user requirements). Track structure simulations require material-specific data, i.e. cross sections describing the interaction of the particles with the molecules of the medium.

To this date, published cross section data for electron impact on some dosimetrically relevant materials, such as constituents of the DNA, are incomplete. Existing data sets are based either on theoretical models (Edel et al., 2006; Sanz et al., 2014), which are valid only in limited energy ranges, or data are available as a patchwork of measured cross sections for some of the DNA constituents in limited energy and angular ranges. In addition, particularly the phosphate group of the DNA has been rarely studied compared to the deoxyribose and nucleobase components. Until now, the most comprehensive data compilation for the deoxyribose-analogue tetrahydrofuran (THF) has been provided by Fuss et al. (2014). They recommend a set of differential elastic cross sections as well as total cross sections (i.e. total scattering, elastic scattering, ionization, rotational, vibrational and electronic exitations) for electrons in a broad energy range, which is mainly based on theoretical data, strengthened by thorough analysis of theoretical and experimental data in the literature. This data set, however, does not contain differential ionization cross sections to take into account the energy loss of the primary electron, the energy of the secondary electron as well as the scattering and emission angles.

Recently, measurements of cross section data of DNA constituents for an impact of electrons with kinetic energies below 1 keV were performed at the PTB (Baek et al., 2012, 2013, 2014; Baek, 2016a, 2016b). In those experiments, cross sections for total scattering were measured for energies between 6 eV and 1 keV, while differential elastic and double-differential inelastic scattering cross sections were measured for energies between 20 eV and 1 keV and scattering angles between 5° (elastic)/15° (inelastic) and 135°. Hence, these measurements provide the most exhaustive, experiment-based and consistent data set for DNA constituents to this date. The DNA constituents of interest were THF, trimethylphosphate (TMP) and PY, serving as models for the deoxyribose and phosphate groups in the DNA backbone as well as for the pyrimidine nucleobases, respectively.

In this work, a cross section data set that would be required for a

* Corresponding author.
E-mail address: marion.bug@ptb.de (M.U. Bug).

http://dx.doi.org/10.1016/j.radphyschem.2016.09.027
Received 11 August 2016; Received in revised form 20 September 2016; Accepted 24 September 2016
Available online 27 September 2016
0969-806X/

simulation of secondary electron transport down to the ionization threshold was developed, consistently based on the data measured at the PTB and taking also into account the available literature data. In addition to the data for THF, TMP and PY, cross sections for purine (PU) as the precursor of the purine nucleobases, are proposed. The propagation of experimental uncertainties to obtain the uncertainties of the model functions is described in Bug (2014). Please note that interactions driven by electrons with very low energies (dominant cross sections at energies below the ionization threshold of about 10 eV) are beyond the scope of this paper as comprehensive reviews are available from the Sherbrooke group (Sanche, 2005; Alizadeh et al., 2015).

In the following, each type of cross section will be discussed individually, i.e. total scattering cross sections (TCS), differential (DelCS) and total (TelCS) elastic scattering cross sections, double-differential (DDCS), single-differential (SDCS) and total (TICS) ionization cross sections and finally, total inelastic and total excitation cross sections. The sections related to each cross section type are structured in the following way: the acquisition of the PTB data is only briefly introduced, followed by a detailed comparison to literature data for each molecule. Finally, the model functions are provided together with a discussion of the selected cross section data. The data set is already used in the track structure code system PTra (Bug, 2014) and is being implemented in the Geant4-DNA toolkit (Incerti et al., 2010).

2. Total scattering cross sections

Total scattering cross sections (TCS) of the DNA constituents THF and PY were measured by Baek et al. (2012, 2013) in a linear transmission device for electrons with impact energies ranging from 6 eV to 1 keV. For those kind of experiments it generally has to be kept in mind that the limited energy and angular resolutions lead to a contribution to the current of unscattered electrons, arising from electrons, scattered in forward direction with a minor energy loss. Such electrons have been scattered elastically or via rotational excitations (and, to a lesser part, vibrational excitations). Their contribution to the detected current leads to a reduced TCS with respect to its true value.

2.1. Comparison to literature data

2.1.1. Tetrahydrofuran (THF)

The linear transmission technique was also deployed by Fuss et al. (2009) (50 eV to 5 keV), Możejko et al. (2006) (1–370 eV) and Zecca et al. (2005) (2–21 eV). On the other hand, Allan (2007) (0.1–20 eV) used electron spectrometry to measure angular-dependent elastic and vibrational excitation cross sections, the sum of which is shown in Fig. 1. The measured TCS of Baek et al. (2012) agree within combined experimental uncertainties with those of Allan (2007), Fuss et al. (2009) and Możejko et al. (2006) but do not show the shoulder around 30–50 eV, present in the data of Możejko et al. (Fig. 1). Only the deviation of the data point of Fuss et al. at 50 eV exceeds the experimental uncertainties as it is 19% larger than the data of Baek et al. (2012). The values of Zecca et al. (2005) are qualitatively similar but systematically lower due to an inferior angular resolution (as stated by Fuss et al. (2009) and Do et al. (2011)).

Theoretical TCS were calculated by Chiari et al. (2013) using the independent atom model – screened additivity rule (IAM-SCAR), where the TCS of the molecule is obtained by summing those of the individual atoms, accounting for the molecular geometry by introducing screening coefficients. Their TCS are in the order of 20% and 30% lower (with and without considering rotational excitations) than the experimental data. Referring to a discussion in their publication regarding the positron TCS calculated by the same approach, this may be a systematic problem in their calculation.

2.1.2. Pyrimidine (PY)

The experimental TCS of Baek et al. (2013) are in good agreement with those recently measured by Fuss et al. (2013) (8–500 eV) only in the energy range above 100 eV (Fig. 1). Towards lower energies, the deviation between both data sets increases to 62% at 8 eV. This discrepancy may arise from the large dipole moment of PY, generally inducing a large contribution of rotational excitations to the TCS and pronounced forward scattering in elastic collisions. Both groups used a linear transmission technique and Fuss et al. additionally applied a strong axial magnetic field which enabled a detection also of electrons scattered in any angle. Electrons with scattering angles larger than the angular resolution were discriminated against the unscattered fraction. As the energy resolution is similar in both experimental setups, the deviation of measured TCS is predominantly attributed to the different angular resolutions of 3.3–14.6° in the experiment of Fuss et al. (2013) and better than 1° for the values of Baek et al. (2013).

The measured TCS of Fuss et al. are supported by theoretical data of different groups (Ferraz et al., 2013; Sanz et al., 2014; Zecca et al., 2010) when the TCS is calculated as in the experimental conditions (without the forward scattered contribution (Fig. 1). The theoretical data were obtained by means of different methods, i.e. of Ferraz et al. (2013) used the scaled quasi-free-scattering model, the IAM-SCAR model was applied by Zecca et al. (2010) and Sanz et al. (2014), complemented by R-matrix calculations by Sanz et al. for energies below 15 eV. A dedicated discussion on the theoretical data and those measured by Fuss et al. can be found in Fuss et al. (2013). For better readability, only the theoretical data of Zecca et al. were selected in Fig. 1.

On the other hand, the experimental TCS of Baek et al. (2013) are only up to 8% lower (above 10 eV) than the theoretical TCS considering the contribution of rotational excitations. This means that the better angular resolution in their experiment enables the measurement of probably the major part of the rotational excitation contribution. As the contribution of rotational excitations can only be quantified theoreti-

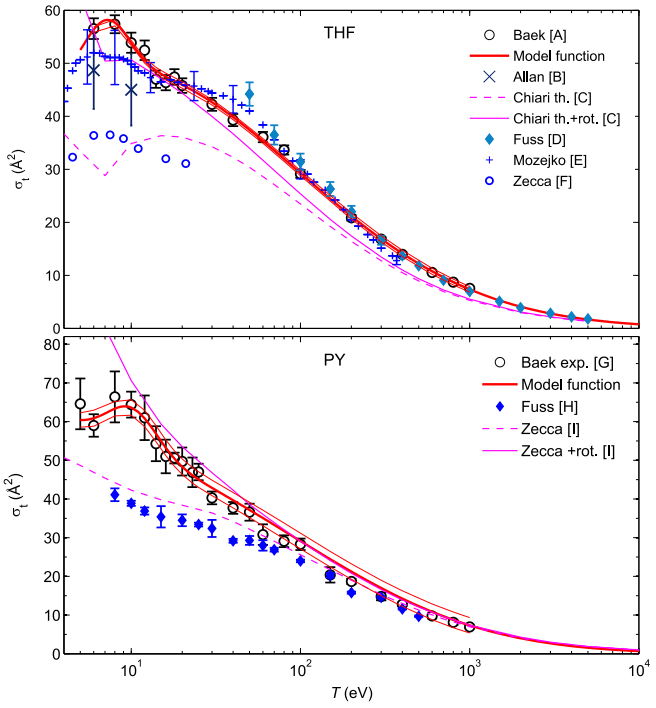

Fig. 1. Measured data and interpolation model curves for total scattering cross sections σ_t of THF and PY as a function of electron energy T, including experimental data of several groups (A Baek et al., 2012; B Allan, 2007; C Chiari et al., 2013; D Fuss et al., 2009 (only statistical uncertainties shown); E Możejko et al., 2006; F Zecca et al., 2005; G Baek et al., 2013; H Fuss et al., 2013; I Zecca et al., 2010). Thin lines indicate the uncertainties of the model functions.

cally, the discrepancies present for the theoretical TCS have to be further investigated.

2.1.3. Trimethylphosphate (TMP) and purine (PU)

TCS for the other DNA constituents of interest in this work, TMP and PU were estimated by a semiempirical approach, where the TCS of a polyatomic molecule is obtained from the sum of the TCS of smaller molecular groups. Among many authors, the applicability of this scaling procedure has been shown for THF and PY by Baek et al. (2012, 2013) and by Domaracka et al. (2008) for polyatomic molecules containing nitrogen or cyclic-ether molecules $(CH_2)_nO$, n=2–4, for electron energies down to 8 eV or 20 eV, respectively. Szmytkowski (1989) showed proportionality between the TCS and the dipole polarizability for various target molecules.

The total scattering cross sections of trimethylphosphate $(CH_3)_3PO_4$ were obtained from the sum of the TCS of submolecular structures $\sigma_{(CH_3)_3PO_4} = \sigma_{(CH_3)_3P} + 2\,\sigma_{O_2}$. The TCS of trimethylphosphine $(CH_3)_3P$ have been measured by Domaracka et al. (2007) for electrons in the energy range between 0.4 and 400 eV using the linear transmission technique. The sum of those data and cross sections of molecular oxygen (Itikawa, 2009) is shown in Fig. 2.

The total scattering cross sections of purine $C_5H_4N_4$ were calculated from the sum $\sigma_{C_5H_4N_4} = \sigma_{C_4H_4N_2} + \sigma_{N_2} + \sigma_{CH_4} - 2\,\sigma_{H_2}$. For pyrimidine $C_4H_4N_2$, the measured data of Baek et al. (2013) were used. Those of molecular nitrogen N_2 were taken from the review of Itikawa (2006), while the data of methane CH_4 have been measured by Sueoka and Mori (1986). The TCS of hydrogen H_2 were taken from the review of Yoon et al. (2008). All data are shown in Fig. 3.

2.2. TCS model function

The TCS were interpolated as a function of primary electron energy T by the superposition of Gaussian functions

$$\sigma_t = \sum_{i=1}^{i_{max}} a_i e^{-\left(\frac{x-b_i}{c_i}\right)^2} \quad (1)$$

with $x = \log_{10} T$ and yielding the parameters specified in Table 1.

The data fit was processed taking into account the consistency requirement that the sum of total cross sections for elastic scattering, ionization and excitation equals the TCS. These individual components will be introduced in detail below. For THF, the model function was fitted to the experimental data published by Baek et al. (2012) and are presented in Fig. 1.

In the case of PY, the model function for the TCS of PY shown in Fig. 1 was not an optimum fit to the experimental data published by Baek et al. (2013), as this would have led to underestimated values for the excitation cross sections (shown below) in the energy region between 25 eV and 800 eV. To obtain consistency within the total cross section data, the slightly higher IAM-SCAR data (Zecca et al., 2010) were used in this energy region for the fitting process. The model function is shown together with the experimental data in Fig. 1.

For TMP, the model function was fitted to the sum of the TCS of its molecular components discussed above (see also Fig. 2).

For PU the situation is similar to the one for PY, the model function is not an optimum fit to the semi-empirical values for PU but slightly overestimates the TCS in the energy region between 50 and 100 eV. The provided model function in Fig. 3 ensures consistency with the total cross sections for the individual processes.

3. Elastic scattering cross sections

3.1. Differential elastic scattering CS

Differential elastic scattering cross sections (DelCS) $d\sigma_{el}/d\Omega(T)$ of THF, PY and TMP were measured at the PTB (Baek et al., 2012, 2014; Baek, 2016a) in a crossed-beam experiment for primary electrons with energies T ranging from 20 eV to 1 keV and scattering angles between 5° and 135° (for THF and energies above 60 eV DelCS were also obtained at 5°). While the DelCS of THF and PY were determined on the absolute scale, those of TMP had to be measured using the relative flow technique as described, for example, by Milosavljević et al. (2005). This was necessary because the TCS of TMP could not measured due to the low vapour pressure. It should be pointed out that a contribution of rotational excitation processes (and also vibrational excitation processes) is partially included (for scattering angles above 5°) when using the crossed-beam technique, due to the finite energy resolution ΔE of the hemispherical energy analyser (the energy resolution was 1.7 eV at 1 keV and the angular resolution was 1.6° and 3° at scattering angles below and above 35°, respectively) (Baek et al., 2012, 2014). This contribution leads to an overestimation of the elastic scattering cross sections, particularly at low scattering angles.

3.1.1. Comparison to literature data

3.1.1.1. Tetrahydrofuran. The DelCS of THF measured by Baek et al. (2012) (see Fig. 4) are mostly in reasonable agreement within experimental uncertainties with those of Allan (2007) (0.1–20 eV, 10–180°), Colyer et al., 2007] (6.5–50 eV, 10–130°), Dampc et al. (2007a) (6–20 eV, 20–180°), Gauf et al. (2012) (0.75–30 eV, 10–130°), Homem et al. (2009) (50–1000 eV, 5–130°) and Milosavljević et al. (2005) (20–300 eV, 10–110°). Among all data, the DelCS of Baek et al. cover the largest range of energies and scattering angles of experimental data in the literature. The DelCS in the literature have been extensively discussed by Baek et al. (2012) and Fuss et al. (2014), hence, only a brief summary is provided here.

The following deviations are observed in magnitude and angular dependence: The data measured by Baek et al. exhibit a shoulder at scattering angles of about 25°, which is supported by the data of Dampc et al., Gauf et al. and Colyer et al. but does not occur in the cross sections of Homem et al. and Milosavljević et al. Therefore, deviations exceeding the experimental uncertainties are observed when compared to the data of Homem et al. at scattering angles between 20° and 35°. For those of Milosavljević et al., deviations become larger with decreasing energy, where their data are up to three times larger at scattering angles below 60° than the DelCS of Baek et al. At 30 eV and 40 eV, the data of Colyer et al. deviate from those of Baek et al. at scattering angles above 120°. At 20 eV, the data of Allan, Colyer et al. and Gauf et al. are about 20% lower at all angles, just exceeding the combined uncertainties. On the other hand, the DelCS of Baek et al. at this energy are in good agreement with those of Dampc et al.

The DelCS of Baek et al. at 20 eV and scattering angles below 20° are supported by the theoretical data of Trevisan et al. (2006), obtained

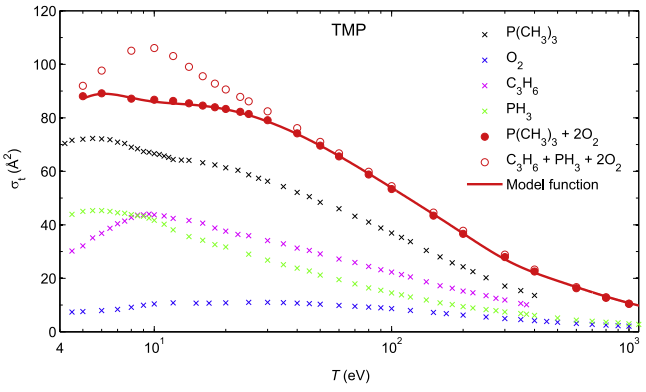

Fig. 2. Total scattering cross sections σ_t of TMP as a function of electron energy T. TMP data were obtained from the experimental data for trimethylphosphine $(CH_3)P$, oxygen O_2, propene C_3H_6 and phosphine pH_3.

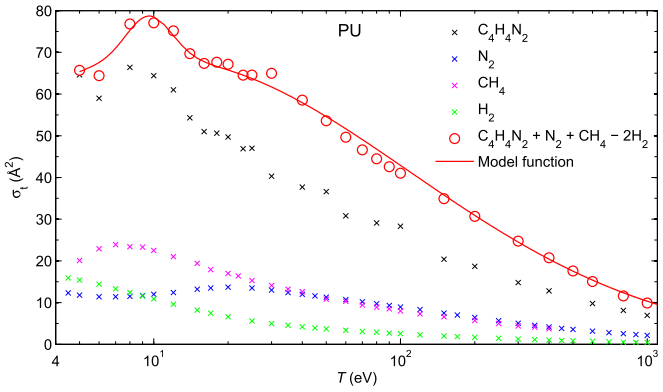

Fig. 3. Total scattering cross sections σ_t of PU as a function of electron energy T. PU data were obtained from the model function for PY $C_4H_4N_2$ and experimental data for nitrogen N_2, methane CH_4 and hydrogen H_2.

by the complex Kohn variational method. Winstead and McKoy (2006) also calculated DelCS of THF for energies 3–50 eV, using the Schwinger multichannel method. At 20 eV, their data support those of Baek et al. for scattering angles above 20°, where those of Trevisan et al. are significantly higher. Theoretical data, calculated by Gauf et al. (2012) using the same method, agree well with their measured data for energies between 6 eV and 20 eV and are in agreement with the data of Baek et al. at 20 eV and large scattering angles. Also the theoretical IAM-SCAR calculations by Fuss et al. (2014) describe the experimental data well within the deviations from each other for all scattering angles and energies between 20 eV and 100 eV. However, they underestimate the DelCS at 1 keV for angles above 40° by about a factor of two. On the other hand, the experimental data of both Baek et al. (2012) and Homem et al. (2009) are well described by theoretical data of both groups, calculated by the IAM method (Homem) and the modified IAM method (MIAM), modified to account for long-range scattering and coherent scattering within the molecule (Baek et al., 2013).

3.1.1.2. Pyrimidine. The DelCS of PY measured by Baek et al. (2013) and shown in Fig. 4 are in good agreement with those measured by Maljković et al. (2009) (50–300 eV, 20–110°) and Palihawadana et al. (2011) (3–50 eV, 10–129°) using a crossed beam experiment and the relative flow method to determine the absolute values. Deviations occur at 30 eV and scattering angles above 110°, where the data of Palihawadana et al. are nearly four times higher. For 200 eV and 300 eV, the data of Maljković et al. are about 40% lower than those of Baek et al. at scattering angles above 100°. The literature data are not shown here as a detailed discussion can be found in Baek et al. (2013).

Calculations of the DelCS of PY were also published by several groups, using the R-matrix method for energies up to 15 eV (Mašín et al., 2012; Sanz et al., 2014), the Schwinger multichannel technique (SMC; Palihawadana et al., 2011), the IAM-SCAR method (Maljković et al., 2009; Palihawadana et al., 2011; Sanz et al., 2014), the MIAM method (Baek et al., 2013) and the scaled quasi-free-scattering model (SQFSM; Ferraz et al., 2013). The list is not complete and the following discussion aims to provide a qualitative overview of the agreement of theoretical and experimental data. More detailed comparisons can be found in Baek et al. (2013), Ferraz et al. (2013), Sanz et al. (2014).

For electron energies between 3 eV and 15 eV, the experimental data of Palihawadana et al. are well described by the R-matrix calculations. The SMC and SQFSM methods reproduce the experimental data well for energies up to 10 eV for all scattering angles, while for 15 eV and 20 eV, the experimental DelCS for angles above 40° are overestimated by approximately a factor of two. At 50 eV, the SMC method provides a good description only for angles up to 30°. On the other hand, the SQFSM method is in excellent agreement with the experimental data up to scattering angles of 60° and slightly overestimates the experiment for larger angles. The IAM-SCAR method perfectly describes the dip in the DelCS between 60° and 110°, but fails particularly at smaller angles. At 100 eV, the IAM-SCAR method is superior to the SQFSM method to describe the experimental data of Maljković et al. (2009), however, the SQFSM method is better describing the experimental data of Baek et al. (2013), which are still in agreement with those of Maljković et al. within the experimental uncertainties. At 300 eV both models are in excellent agreement with the data of Maljković et al. (2009), while the MIAM model better describes the experimental data of Baek et al. (2013).

It is interesting to notice in Fig. 4 that the DelCS of PY are mostly similar to those of THF within combined uncertainties. A good agreement of angular dependences when molecules possess similar shapes, electronic properties and dipole polarizabilities was demonstrated by Palihawadana et al. (2012) for benzene, pyrimidine and pyrazine. In contrast to pyrimidine, benzene and pyrazine have no dipole moment, but Palihawadana et al. measured very similar DelCS for all three molecules in the energy region 10–50 eV and scattering angles 10–129°. This implies that dipole properties of the molecules have no significant impact on DelCS above 10° scattering angle.

3.1.1.3. Trimethylphosphate. In Fig. 5, DelCS of TMP (Baek, 2016a) are compared with those of THF where the latter are multiplied by the ratio of the number of valence electrons in both molecules. Due to the different molecular shapes, the angular dependence of the data slightly differs for both molecules, with a lower probability of forward scattering from THF relative to TMP for energies below 100 eV and a lower probability for large-angle scattering from THF relative to TMP in the higher energy range.

3.1.1.4. Purine. The DelCS of PU were determined from those of the other DNA constituents used in this work (THF, PY and TMP). Literature data of the DNA nucleobases adenine, cytosine, guanine and thymine were also taken into account. Such data were calculated by Możejko and Sanche (2003) (50–4000 eV) by the independent atom model as well as by Blanco and García (2009) (5 eV–10 keV) using the IAM-SCAR method. Both groups found a similar angular dependence (within 3%) for the four nucleobases, while the absolute values of the elastic scattering cross sections were proportional to the molecular weights (Możejko and Sanche, 2003; Blanco and García, 2009). They concluded that the elastic scattering cross section mainly depends on the molecular size and the number of atoms in the molecule rather than on differences in the molecular geometries between pyrimidine and purine bases. In fact, the dipole polarizabilities of DNA nucleobases are generally large and differ by 30%, so that an effect on the DelCS seems

Table 1
Parameters used in Eq. (1) to fit the total scattering cross sections of THF, PY, PU and TMP.

	a_1 (Å^2)	b_1	c_1	a_2 (Å^2)	b_2	c_2	a_3 (Å^2)	b_3	c_3
THF	9.206	0.856	0.184	49.04	0.911	1.517			
PY	9.854	1.008	0.204	40.45	1.164	1.406	38.890	−0.038	1.023
PU	10.33	0.980	0.130	68.42	1.012	1.446			
TMP	10.47	0.712	0.218	84.82	1.116	1.311	−1.785	2.498	0.205

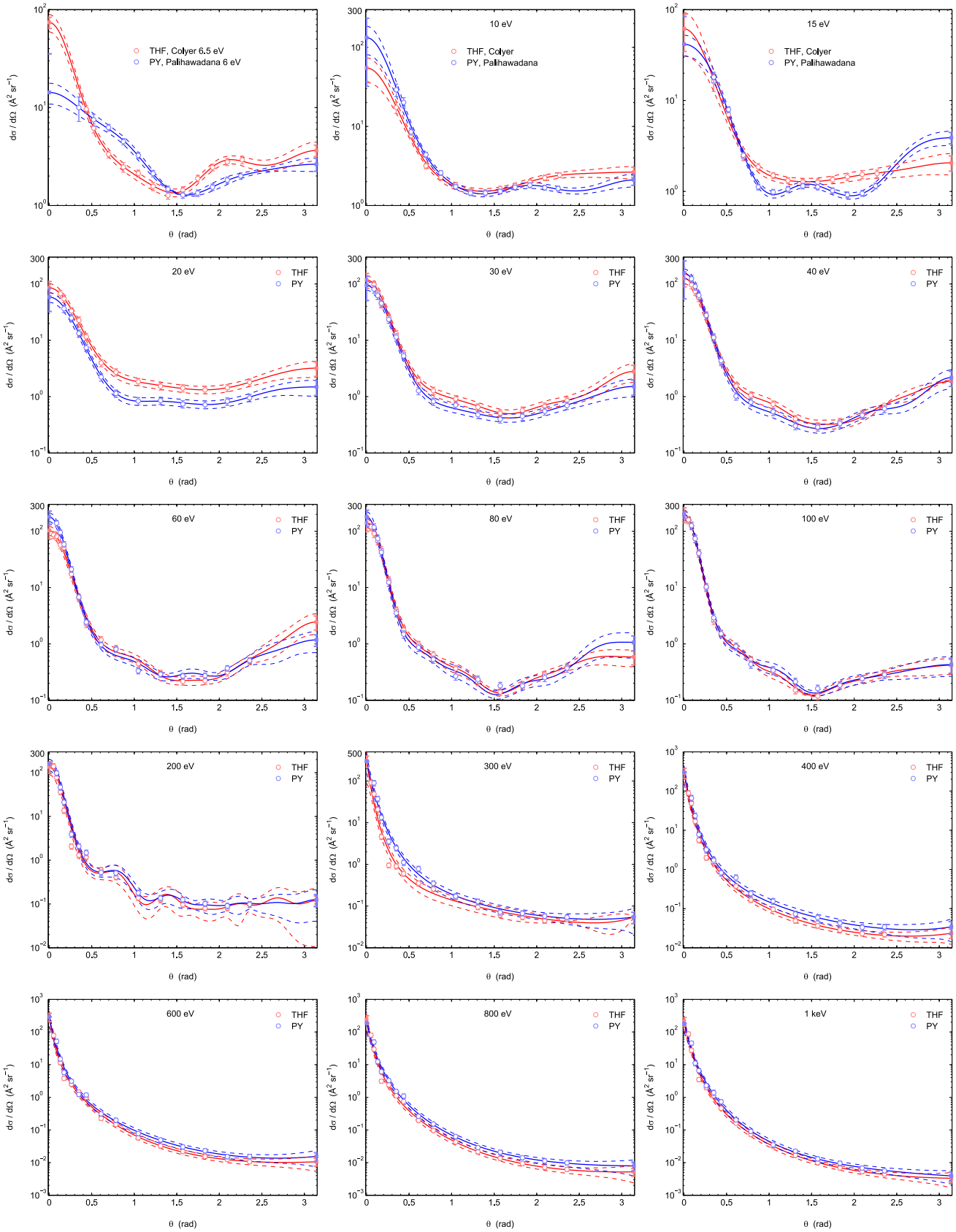

Fig. 4. DelCS of THF and PY as function of scattering angle. Measured data are shown as well as the curves obtained from the best fit. Dashed lines indicate the uncertainties of the fit. Filled squares show the extrapolated values (see text).

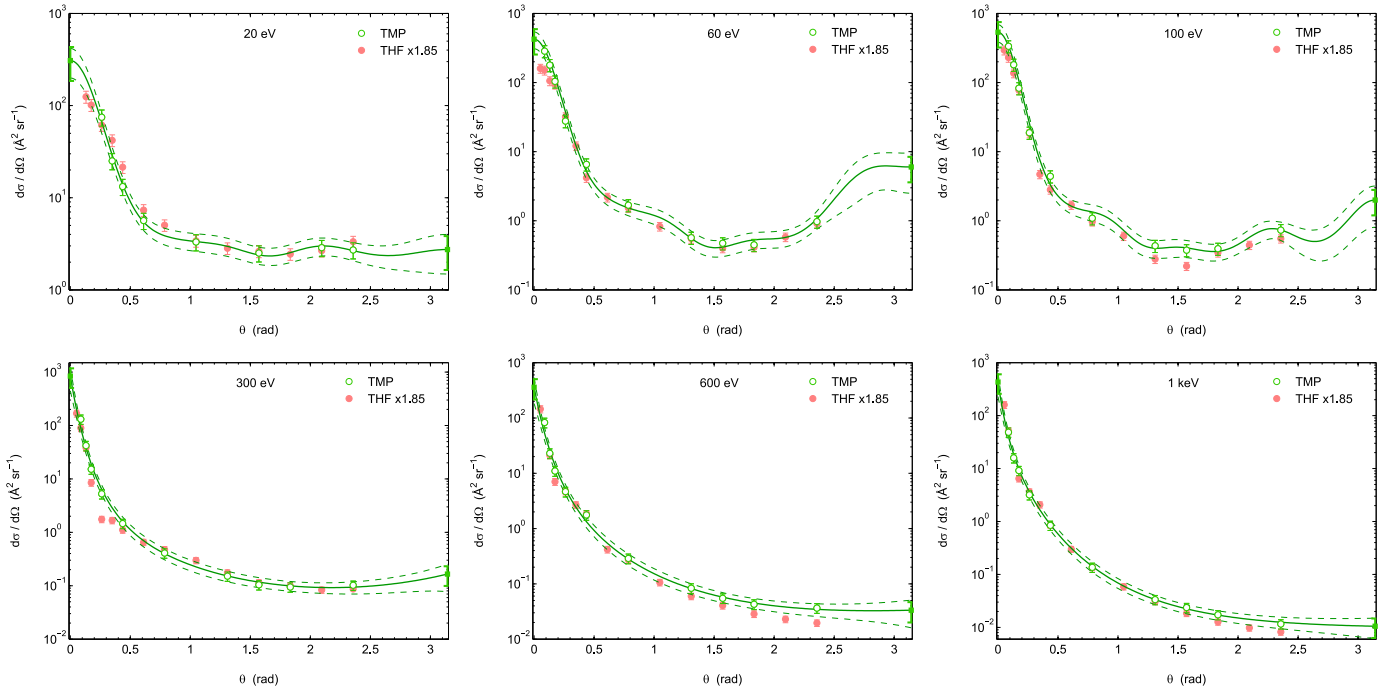

Fig. 5. DelCS of TMP as function of scattering angle. Measured data and the curves obtained from the best fit are shown. Dashed lines indicate the uncertainties of the fit. Filled squares show the extrapolated values (see text). THF data are presented again for comparison.

to be negligible. Based on those findings, the angular dependence of elastic scattering cross sections for pyrimidine was also used for purine. The absolute values of the DelCS of PU were calculated by multiplying the DelCS of PY by the ratio of total scattering cross sections. As the total scattering cross sections are proportional to the molecular weights and the nucleobases consist of low-Z atoms, the uncertainty arising from this scaling procedure is negligible.

3.1.2. DelCS model functions

For the application in track structure simulation codes, the model function has to provide an interpolation of the measured data as a function of the scattering angle as well as an extrapolation to 0° and 180°. For the fit of the model function, the measured data of Baek et al. (2012, 2014) were complemented by the DelCS of THF by Colyer et al. (2007) (6.5–50 eV, 10–130°) for electron energies between 6.5 eV and 15 eV, while the data of Palihawadana et al. (2011) (3–50 eV, 10–129°) were used between 3 eV and 15 eV for PY. In the overlapping energy ranges, the data of both groups are in good agreement with those measured by Baek et al. (2012, 2014).

In the lower energy range (up to 200 eV), the molecular phase-shift analysis technique was applied to fit the measured DelCS via parameters δ_l and N, related to the phase shift and the amplitude, respectively. This model was previously suggested by Tanaka et al. (1982). In the description of the scattering amplitude (ICRU, 2007), δ_l are the phase shifts which have to be used as fitting parameters in this procedure. In this work, the fit was performed to the logarithm of the DelCS, as the determination of suitable starting parameters was less time consuming due to the smaller range of the data. In fact, Eq. (2a) was applied (DelCS in units Å^2 sr^{-1}), using partial waves with l_{max} between 5 and 7. A higher number of partial waves was unnecessary in this energy range. For energies of 300 eV and above, an appropriate number of parameters would have led to an overdetermined problem (only 13 or 14 data points are available from the measurements). However, the interference of a large number of partial waves effectively results in an exponential decrease of the DelCS with increasing scattering angle. Therefore, the angular dependence for higher energies was approximated by using a superposition of exponential functions as given in Eq. (2b) (DelCS in units Å^2 sr^{-}).

$$\log_{10}\left(\frac{d\sigma_{el}}{d\Omega}\right)(T < 300\ \text{eV}) = N\left|\sum_{l=0}^{l_{max}}(2l+1)(e^{2i\delta_l}-1)P_l(\cos\theta)\right|^2 - C \tag{2a}$$

$$\log_{10}\left(\frac{d\sigma_{el}}{d\Omega}\right)(T \geq 300\ \text{eV}) = \sum_{j=1}^{3} a_j e^{-b_j\times\theta} - C \tag{2b}$$

The extrapolation of the DelCS to all scattering angles was performed as follows. Both models required the specification of the value at 180°, which was estimated using the available theoretical data. Below 200 eV, the phase-shift analysis technique provided a reasonable extrapolation to 0° while for higher energies the extrapolated values appeared too high due to the character of the exponential model function. Hence for those energies, the extrapolated value at 0° was estimated beforehand. Generally, the extrapolation to forward scattering angles is a sensitive procedure, as the contribution to the integral of the DelCS is significant. Also, the contribution of rotational excitations is large at forward angles and can only be obtained by theoretical models (Baek et al., 2013; Fuss et al., 2013). Under those circumstances, the extrapolation was performed with the condition that the total elastic scattering cross section is a continuously decreasing function of the electron energy (Section 3.2). Uncertainties of the extrapolated data points at 0° and 180° were conservatively estimated to be twice as large as the uncertainties at 15° and 135°, respectively.

The model functions for the DelCS of THF, PY and TMP are shown in Figs. 4 and 5. Parameters for the model functions are provided in Table 2 for THF, PY and TMP, while those of PU could be scaled based on the data of PY (see above). At energies up to 100 eV, the molecular phase-shift analysis technique (Eq. (2a)) provides a good representation of the measured data. This model well describes the structures occurring in the intermediate angular range of the DelCS. At 200 eV and scattering angles above 60°, the magnitude of oscillatory structures (which would vanish for a larger number of partial waves) is within the experimental uncertainties.

Table 2
Parameters to calculate the DelCS of THF, PY and TMP via Eqs. (2a) and (2b) for electrons of energy T. Numbers in parentheses indicate the order of magnitude.

Tetrahydrofuran

T (eV)	N	δ_0	δ_1	δ_2	δ_3	δ_4	δ_5	δ_6	δ_7	C
6.5	5.458(−2)	−8.497(−1)	6.803(−1)	1.054(−1)	−5.925(−3)	−3.101	−3.100			0
8	6.275(−2)	−8.533(−1)	5.721(−1)	1.459(−1)	1.975(−2)	−3.120	−3.124			0
10	5.742(−2)	−8.446(−1)	6.023(−1)	1.497(−1)	3.953(−2)	−3.119	−3.134			0
15	2.785(−1)	−1.319	2.428(−1)	6.475(−2)	2.640(−2)	−3.132	−3.138			1
20	2.908(−1)	−1.422	2.176(−1)	3.395(−2)	3.991(−2)	−3.126	−3.139			1
30	1.903(−1)	−1.363	3.339(−1)	1.085(−2)	2.794(−2)	−3.108	−3.119			1
40	2.559(−1)	1.037	−3.080	−3.022	3.142	−5.683(−3)	1.751(−2)	1.336(−2)		1
60	2.028(−1)	1.008	−3.080	−2.986	3.132	−1.188(−2)	2.151(−2)	1.987(−2)		1
80	5.357(−2)	9.535(−1)	−8.949(−1)	3.142	3.622(−2)	−7.055(−2)	−8.254(−2)	3.104	−1.069(−3)	1
100	3.560(−2)	7.860(−1)	−1.169	3.068	9.831(−2)	−8.300(−2)	−1.086(−1)	3.065	−1.534(−2)	1
200	2.464(−1)	1.633	−1.452(−1)	2.995	−2.831(−2)	1.422(−2)	3.215(−2)	3.142	−4.765(−2)	2

	a_1	b_1	a_2	b_2	a_3	b_3				
300	1.801	4.694(−1)	2.683	4.962	3.334(−5)	−2.927				2
400	2.672	9.992(−1)	1.795	5.772	9.684(−4)	−1.775				2
600	3.824	1.002	1.319	9.832	3.224(−1)	−3.127(−1)				3
800	3.842	9.615(−1)	1.394	7.619	1.454(−1)	−4.107(−1)				3
1000	3.656	9.518(−1)	1.575	5.875	1.003(−1)	−3.850(−1)				3

Pyrimidine

T (eV)	N	δ_0	δ_1	δ_2	δ_3	δ_4	δ_5	δ_6	δ_7	C
3	4.736(−2)	−1.833	5.419(−1)	−2.307(−1)	−7.889(−2)	−3.127	−3.149			0
6	3.281(−2)	−1.171	9.261(−1)	−5.013(−2)	−1.437(−1)	−3.174	−3.142			0
10	3.383(−2)	−8.830(−1)	8.237(−1)	2.545(−1)	4.911(−2)	−3.130	−3.109			0
15	2.577(−1)	−1.152	3.053(−1)	8.500(−2)	5.050(−2)	−3.148	−3.152			1
20	2.241(−1)	−1.272	2.621(−1)	7.646(−2)	5.297(−2)	−3.129	−3.143			1
30	1.707(−1)	−1.291	3.312(−1)	4.326(−2)	5.031(−2)	−3.109	−3.129			1
40	4.034(−1)	7.320(−1)	−3.110	−3.068	3.157	5.087(−3)	6.140(−3)	1.092(−2)		1
60	1.576(−1)	1.223	−3.060	−2.952	3.142	−2.166(−2)	3.241(−2)	2.542(−2)		1
80	4.977(−2)	7.982(−1)	−9.712(−1)	3.141	2.494(−2)	−5.332(−2)	−1.012(−1)	3.088	1.740(−3)	1
100	4.310(−2)	9.694(−1)	−9.621(−1)	3.115	6.731(−2)	−6.296(−2)	−1.045(−1)	3.084	−1.261(−2)	1
200	2.682(−1)	1.661	−1.563(−1)	3.029	−3.022(−2)	1.669(−2)	2.323(−2)	3.132	−3.700(−2)	2

	a_1	b_1	a_2	b_2	a_3	b_3				
300	2.037	5.396(−1)	2.431	3.531	7.004(−3)	−1.255				2
400	2.401	7.413(−1)	2.076	4.753	1.029(−3)	−1.807				2
600	3.608	7.009(−1)	1.756	6.057	1.006(−1)	−6.562(−1)				3
800	3.779	1.059	1.051	6.745	4.468(−1)	−1.708(−1)				3
1000	3.345	1.366	9.677(−1)	6.147	9.452(−1)	1.741(−1)				3

Trimethylphosphate

T (eV)	N	δ_0	δ_1	δ_2	δ_3	δ_4	δ_5	δ_6	δ_7	C
20	3.460(−1)	−1.514	1.802(−1)	2.572(−2)	5.956(−3)	−3.112	−3.121			1
30	3.018(−1)	−1.392	2.749(−1)	−1.966(−2)	3.935(−3)	−3.100	−3.115			1
40	2.608(−1)	−1.328	3.379(−1)	−8.721(−4)	−4.354(−3)	−3.123	−3.113	1.727(−2)		1
60	1.729(−1)	−1.192	4.677(−1)	−7.736(−3)	3.978(−3)	−3.130	−3.103	2.680(−2)		1
80	2.553(−1)	1.178	−3.114	−2.999	3.172	−1.802(−2)	−5.022(−3)	1.514(−2)	1.990(−2)	1
100	1.410(−1)	1.189	−4.679(−1)	3.070	−7.398(−4)	−1.725(−3)	−1.199(−2)	3.121	−2.938(−2)	1
200	3.524(−1)	−1.617	1.752(−1)	6.046(−2)	2.975(−2)	−3.132	−3.167	−2.318(−3)	3.785(−2)	2

	a_1	b_1	a_2	b_2	a_3	b_3				
300	2.554	7.971(−1)	2.258	5.097	1.123(−1)	−6.989(−1)				2
400	2.777	9.971(−1)	1.837	6.313	2.396(−1)	−4.054(−1)				2
600	3.176	1.053	1.437	5.655	9.429(−1)	−1.276(−1)				3
800	3.510	1.181	1.288	9.607	8.628(−1)	−9.270(−2)				3
1000	3.707	1.438	9.801(−1)	1.053(+1)	9.466(−1)	−1.151(−2)				3

3.2. Total elastic scattering CS

Total elastic scattering cross sections (TelCS) were obtained by numerical integration of the model function obtained in the previous section over all scattering angles.

The total elastic scattering cross section is very sensitive to the extrapolation of the DelCS to forward angles, particularly for polar molecules such as THF or PY. For example, the TelCS of THF increases up to 30% when the DelCS is extrapolated by the model functions instead of assuming a plateau between 0° and 5°. It should be noted that this effect occurred even though the DelCS is 'weighted' by the sine of the scattering angles by which the contribution of forward scattering is of less importance than for intermediate scattering angles.

3.2.1. Comparison to literature data

3.2.1.1. Tetrahydrofuran. The TelCS of THF determined in this work are between 5% and 25% higher than the values given previously by Baek et al. (2012) (see Fig. 6), as Baek et al. performed the integration of the same data set only between 3° and 180°. The TelCS in this work are in good agreement within the uncertainties with measured data of Allan (2007) (0.1–20 eV), Colyer et al. (2007) (6.5–50 eV), Gauf et al. (2012) (0.75–30 eV) and Homem et al. (2009) (50–1000 eV) for energies above 8 eV. The relatively low value of the TelCS at 300 eV (in this work or given in Baek et al., 2012) seems to be caused by an underestimated DelCS for scattering angles between 4° and 40°. This is supported by the fact that the DelCS of THF and PY are generally similar for energies above 100 eV. Below 8 eV, the TelCS of Gauf et al. (2012) are nearly a factor of two larger than those of Allan (2007) and Colyer et al. (2007).

When comparing experimental TelCS to theoretical data it should be kept in mind that the experimental data contain a significant contribution of rotational excitation as such electrons cannot be resolved due to the limited energy resolution in the experiment. This has already been supported in several publications (Winstead and McKoy, 2006; Fuss et al., 2014) where it was observed that the theoretical data including a Born-dipole correction to account for rotational excitations reproduce the DelCS and TelCS better than theoretical data without the Born-dipole correction.

Calculations of elastic cross sections were performed by Fuss et al. (2009, 2014) (1 eV to 10 keV) using the IAM-SCAR method, which considers rotational excitations within the TelCS. In their most recent publication (Fuss et al., 2014), the total cross sections applied in the code LEPTS are provided with a rigorous distinction between the TelCS and the rotational excitation cross section. Their recommendations are based on the good agreement of their IAM-SCAR data at energies above 20 eV with experimental data and the excellent description of experimental data at lower energies by the Schwinger multichannel calculations of Winstead and McKoy (2006) (not shown), who also provide the same data without the Born-dipole correction applied. The TelCS of Fuss et al. (2014) as well as the sum of both elastic and rotational excitation cross sections are shown in Fig. 6. At energies above 1 keV, the sum of both cross sections is 5% higher than their recommended TelCS and the difference is increasing to 25% at 10 eV and a factor of two at 1.5 eV. Hence, both curves are good descriptions of the experimental data within the experimental uncertainties at energies above 30 eV. At 20 eV and below, the TelCS based on the DelCS of Baek et al. and Gauf et al. seem to contain a higher contribution of rotational excitations than the TelCS calculated by Allan and Colyer et al. TelCS were also calculated by Możejko and Sanche (2005) (50–2000 eV) by the IAM model. Their TelCS have a different energy dependence with a steeper slope at energies below 1 keV than the data of the other authors, leading to higher values at 50 eV by 35% when compared to the data of Fuss et al. including rotational excitations.

3.2.1.2. Pyrimidine. TelCS of PY were determined by Palihawadana et al. (2011) (3–50 eV) from measured DelCS using extrapolation by the molecular phase shift method (Tanaka et al., 1982). As their DelCS data were used in this work at energies below 20 eV with a similar extrapolation method, good agreement with TelCS in this work is observed (Fig. 7). Both data sets agree up to 50 eV. The integration of the theoretical DelCS was shown by Mašín et al. (2012) to yield excellent agreement with experimental data if the integration was performed only over the limited range of scattering angles covered in the experiment. This is explainable, as the extrapolation of the experimental data to forward angles is particularly difficult for molecules with large dipole moments, leading to a large non-resolved contribution of rotational excitations.

Comparing the TelCS obtained after integration of DelCS over all scattering angles, it can generally be observed that in the energy range up to 20 eV, the TelCS calculated by the R-matrix theory (Mašín et al., 2012; Sanz et al., 2014) or the IAM-SCAR method (Sanz et al., 2014) agree well with the TelCS obtained from the experiments (Baek et al., 2014; Palihawadana et al., 2011) if no Born-dipole correction is applied. In the energy range 30 eV and above, the contribution of rotational excitations is lower and the experimental data are well reproduced if the Born-dipole correction is applied in the theoretical data. The best description of the experimentally-based TelCS, however, is obtained by the SMC theory applied by Palihawadana et al. (2011). In Fig. 7, the TelCS recommended by Sanz et al. (2014) (calculated with the Born-dipole correction) is shown exemplarily, while a more detailed summary of the theoretical data can be found in their publication.

3.2.1.3. Trimethylphosphate. As no experimental data of TMP are available in the literature, the data are compared to those of trimethylphosphine $P(CH_3)_3$, calculated by Domaracka et al. (2007) using the IAM approach. Their data, multiplied by the ratio of the number of electrons in both molecules, also shown in Fig. 7, are in excellent agreement with our TelCS values in the energy range between 30 and 1000 eV.

3.2.1.4. Purine. The TelCS of PU were determined by multiplying those of PY with the ratio of total scattering cross sections in accordance with the procedure applied for the DelCS of PU.

3.2.2. TelCS model functions

The integrated DelCS were fitted by the following model functions,

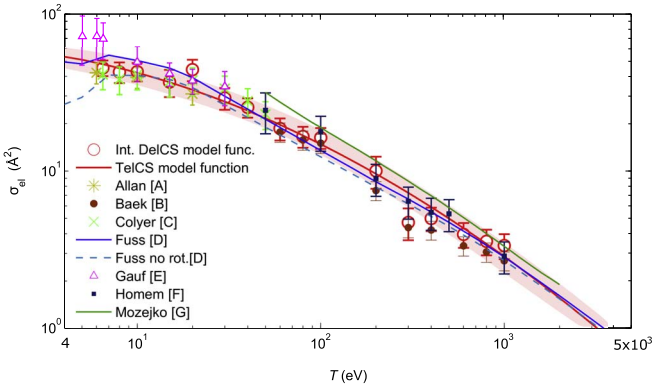

Fig. 6. TelCS determined by integrating the DelCS model functions of THF and the model function for the TelCS. Uncertainties of the model function are shown as shaded area. Literature data are also shown (A Allan, 2007; B Baek et al., 2012; C Colyer et al., 2007; D Fuss et al., 2014; E Gauf et al., 2012; F Homem et al., 2009; G Możejko and Sanche, 2005).

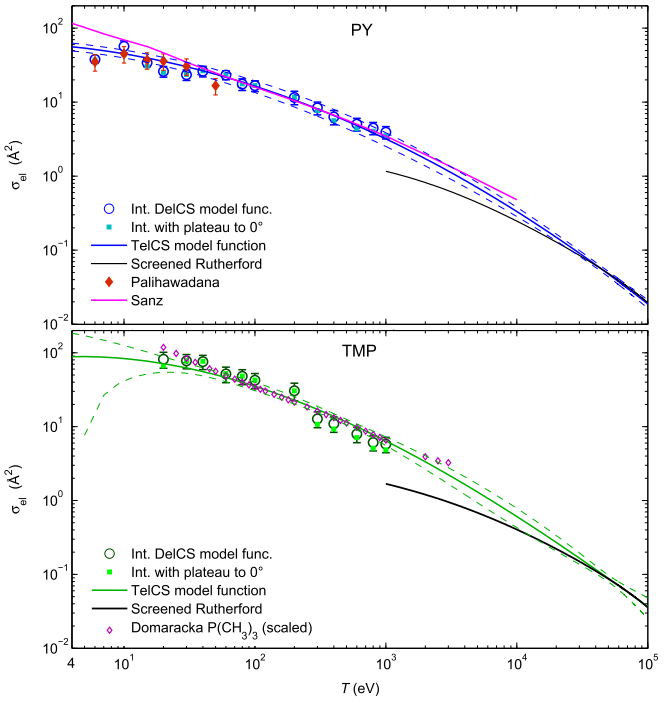

Fig. 7. TelCS determined by integrating the DelCS model functions of PY and TMP and the respective model functions for the TelCS. Literature data of Palihawadana et al. (2011) and Domaracka et al. (2007) are also shown.

also shown in Figs. 6 and 7

$$\log_{10}(\sigma_{el}) = a[\log_{10}(T)]^b + c, \tag{3a}$$

$$\log_{10}(\sigma_{el}) = \sum_{i=0}^{3} d_i[\log_{10}(T)]^i \tag{3b}$$

where σ_{el} is in units of Å^2 and T is in eV. The parameters are provided in Table 3. Eq. (3a) was used for THF and PY while a polynomial function was applied for TMP to satisfy the consistency requirements at low and high-energy limits: at low energies, the TelCS is restricted by the total scattering cross section. In the high-energy limit, the TelCS were calculated by the screened Rutherford formula (given, for example, in references Grosswendt and Waibel, 1978; Uehara et al., 1992) which appears to provide a physically meaningful extrapolation to energies above 50 keV.

The TelCS model functions, fitted to the integrated DelCS by Eq. (3a), are up to 12% larger for PY than those of THF with maximum deviations in the energy region between 100 eV and 1 keV. This is in agreement with the larger number of electrons in the molecule (42 for PY, 40 for THF).

The model function for the TelCS of TMP also describes the experimental data well within the uncertainties for all energies between 20 and 1000 eV (Fig. 7). Towards 20 eV and 3 keV however, the data of Domaracka et al. become larger than those predicted by the model function. This behaviour has already been observed for the THF data, calculated by Możejko and Sanche (2005) using the same theoretical approach as Domaracka et al.

4. Ionization cross sections

4.1. Double-differential ionization CS

Double-differential inelastic cross sections were determined at the PTB (Baek, 2016b) using the same crossed-beam arrangement as used in the measurement of the DelCS, described in detail by Baek et al. (2012, 2014). The data of THF and PY were determined on the absolute scale, while those of TMP were measured by the relative flow technique.

Generally, the measured double-differential spectra produced by electrons of initial energy T consist of two parts; according to convention, the spectrum below an energy of $(T - B_0)/2$ (B_0 denotes the binding energy of the outermost shell of the target molecule) arises from the emission of secondary electrons with energy E, while at higher energies an energy loss spectrum of the primary particles is recorded. K-edges and the respective Auger-electron emission peaks for carbon, nitrogen and oxygen as well as Auger-electron emission after phosphorus L-shell ionization in TMP are distinct features in the measured spectra, which have to be separated from the measured spectra to obtain the double-differential cross sections (DDCS) for direct ionization. For this purpose, the DDCS were interpolated in the region of the Auger peaks by fitting spline functions to the experimental spectra as a function of secondary electron energy. An example is shown in Fig. 8.

4.1.1. Comparison to literature data

Up to this date, the only available electron-impact DDCS in the literature have been calculated by Champion (2014) by quantum mechanical calculations within the framework of the first Born approximation. In this approach, the incident and scattered electrons are described by plane waves while the ejected electron is described by a Coulomb wave and experiences an effective ionic target charge. Although the theory did not match the experimental data on a quantitative scale, the general trend of the angular and energy dependencies is reproduced. However, low-angle scattering is significantly overestimated while backscattering is underestimated by the theory.

4.1.2. DDCS model functions

Analytical descriptions of the DDCS as a function of the emission angles are required to extrapolate the measured data to 0° and 180° emission angles. For this reason, the spline-interpolated DDCS (Fig. 8) were fitted as function of the polar emission angle θ. The following model functions are proposed: For primary electron energies T up to 200 eV, superpositioned Legendre polynomials up to fifth degree, described by

$$\frac{d^2\sigma}{dE d\Omega} = \sum_{i=0}^{5} p_i P_i(\cos\theta), \tag{4}$$

are suitable, as Legendre polynomials constitute a term in the quantum mechanical description of the scattering amplitude. Here, p_i are the fitting parameters and P_i the Legendre polynomials of i-th degree. For energies T of 300 eV and above, a formula developed by Rudd (1991) is applied, given by

$$\frac{d^2\sigma}{dE d\Omega} = a_1\left[\frac{1}{1+\left(\frac{cos\theta - a_2}{a_3}\right)^2} + \frac{a_4}{1+\left(\frac{\cos\theta + 1}{a_5}\right)^2}\right] \tag{5}$$

with parameters $a_1 - a_5$. The motivation for using this model was given by Rudd (1991), who observed that the binary encounter peak can be

Table 3
Parameters for the model function for the TelCS in Eqs. (3a) and (3b).

	a	b	c	
THF	−0.169	1.882	1.793	
PY	−0.153	1.952	1.806	
	d_0	d_1	d_2	d_3
TMP	1.921	0.188	−0.220	9.510×10^{-3}

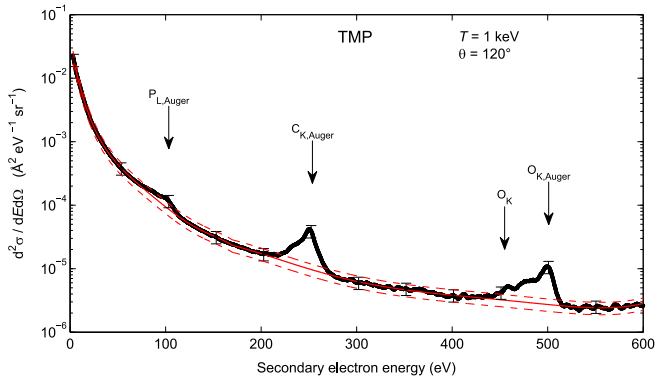

Fig. 8. Spline fit (red) to experimental data (black) of TMP for electrons with energy T of 1 keV and an emission angle of secondary electrons of 120°. Dashed red lines indicate the uncertainties of the spline function. Uncertainties of the experimental data are shown for selected data points. (For interpretation of the references to color in this figure legend, the reader is referred to the web version of this article.)

described by a Lorentzian function; a second Lorentzian function accounts for a backscatter peak. Experimental data measured at angles below 25° were omitted in the fitting procedure as these are likely to be overestimated in the experiment, as has been discussed by Bolorizadeh and Rudd (1986). A selection of DDCS is shown in Fig. 9.

Emission angles calculated by a kinematic model (Grosswendt and Waibel, 1978) and indicated in Fig. 9 provide approximately the mean emission angle determined from the experimental data. It should be noted that the secondary electron emission from THF, PY and TMP is nearly isotropic for secondary electron energies below 15 eV (magnitude varies by less than 20%).

When comparing the DDCS of THF, PY and TMP, the same angular dependence is observed for all molecules. The absolute DDCS of THF and PY are in agreement within combined experimental uncertainties for the entire range of energies and emission angles, which is expected as both molecules have the same number of valence electrons and similar molecular geometries.

4.1.2.1. Purine. Due to the lack of data for the DDCS of PU and the similarity of the molecular structures of PY and PU, it was decided to use the angular dependence of PY. Hence, the absolute values of the DDCS of PU were obtained by scaling the DDCS of PY by the ratio of the total scattering cross sections for PU to those of PY.

4.2. Single-differential ionization CS

The single differential ionization cross sections (SDCS) $\mathrm{d}\sigma_{\mathrm{ion}}/\mathrm{d}E$ were determined by integrating the DDCS model functions over polar and azimuth emission angles θ and ϕ by

$$\frac{\mathrm{d}\sigma_{\mathrm{ion}}}{\mathrm{d}E}(T) = \int_0^{2\pi}\int_0^{\pi} \sin\theta \frac{\mathrm{d}^2\sigma}{\mathrm{d}E\mathrm{d}\Omega}\mathrm{d}\theta\mathrm{d}\phi. \tag{6}$$

In this context, it is interesting to notice a reduction in the SDCS by less than 5% when the integration is only over the angular range of the experiment (between 15° and 135°).

4.2.1. SDCS models from literature

For a convenient implementation in the simulation code and to obtain an extrapolation of the SDCS to 0 eV secondary electron energy, appropriate model functions are required. Theoretical models are available in the literature: Thomson and Mott cross sections (Llovet et al., 2014; ICRU, 1996) provide accurate SDCS for large energy transfers with respect to the electron energy and, hence, can be used to benchmark the SDCS in this energy region. The Binary-Encounter-Bethe (BEB) model, on the other hand, combines the binary-encounter theory with the Bethe-Born approximation, which are expected to be realistic models for collisions with high and very low momentum transfer, respectively. The suitability of these models for the SDCS of THF, PY and TMP is discussed in the following.

4.2.1.1. Thomson and Mott cross sections. The Thomson and Mott cross sections (Llovet et al., 2014; ICRU, 1996) are useful to examine the behaviour of the SDCS for large energy transfers $E_{\mathrm{Tr}} = E + B$ where $E \gg B$. The Thomson cross section for electron impact is the pendant to the Rutherford cross section for proton impact (Llovet et al., 2014). It is obvious from Fig. 10 that both models agree reasonably well with the data derived from the experiment for energies $T > 80$ eV and $E > 50$ eV. While the Thomson cross sections continuously decrease with increasing energy E, the Mott data form a plateau of the SDCS at large E which is accompanied by a steeper slope at energies above 10 eV, originating from the interference between direct ionization and exchange interactions.

4.2.1.2. BEB model. The BEB model (Kim and Rudd, 1994; Hwang et al., 1996) describes the electron-impact ionization cross section without requiring empirical parameters. The SDCS is given by

$$\frac{\mathrm{d}\sigma_{\mathrm{ion}}}{\mathrm{d}E} = \sum_i \left(\frac{S_i}{B_i(t+u+1)} \sum_{n=1}^{3} F_n[f_n(w) + f_n(t-w)] \right), \tag{7}$$

where

$$F_1 = -\frac{F_2}{t+1}, \quad F_2 = 2 - Q, \quad F_3 = Q\ln t \tag{8}$$

and

$$f_n(w) = (w+1)^{-n}, \quad f_n(t-w) = (t-w)^{-n} \tag{9}$$

with $t = T/B_i$, $u = U_i/B_i$, $w = E/B_i$ and $S_i = 4\pi a_0^2 N_i (R/B_i)^2$. R is the Rydberg constant, a_0 is the Bohr radius, B_i and U_i are the binding and kinetic energies of electrons occupying the i-th subshell of the molecule and N_i is the number of electrons in this subshell. The factor Q can be set to unity when the oscillator strength distribution for the molecule of interest is unknown (Kim and Rudd, 1994).

The BEB model, used with the parameters B_i and U_i given in Table 6, is found to generally underestimate the SDCS at low secondary electron energies. As seen in Fig. 10, the integrated experimental data are between 8% and 41% larger at E=3 eV for PY and between 31% and 67% at 2.7 eV for THF data at primary electron energies between 30 eV and 1 keV. For TMP, the BEB model data are 40–50% lower at E=3 eV than the integrated experimental values for primary electron energies 40–200 eV while good agreement is present for higher energies T. Furthermore, the slope of the BEB model predictions as function of secondary electron energy is lower than the slope of the experimental data. Hence, the BEB model underestimates the experimental data at energies E below 25 eV and overestimates the SDCS at intermediate secondary electron energies by up to 45% for THF, 20% for PY and 50% for TMP. At the highest secondary electron energies, the BEB model data are mostly similar to the experimental SDCS of THF, PY and TMP.

4.2.2. SDCS model function

4.2.2.1. Tetrahydrofuran, pyrimidine and trimethylphosphate. A fit of the BEB model to the data obtained by Eq. (6) was applied to improve the agreement with the experimental data, particularly at low secondary electron energies where the SDCS are largest. In this case, Eqs. (7) and (8) become

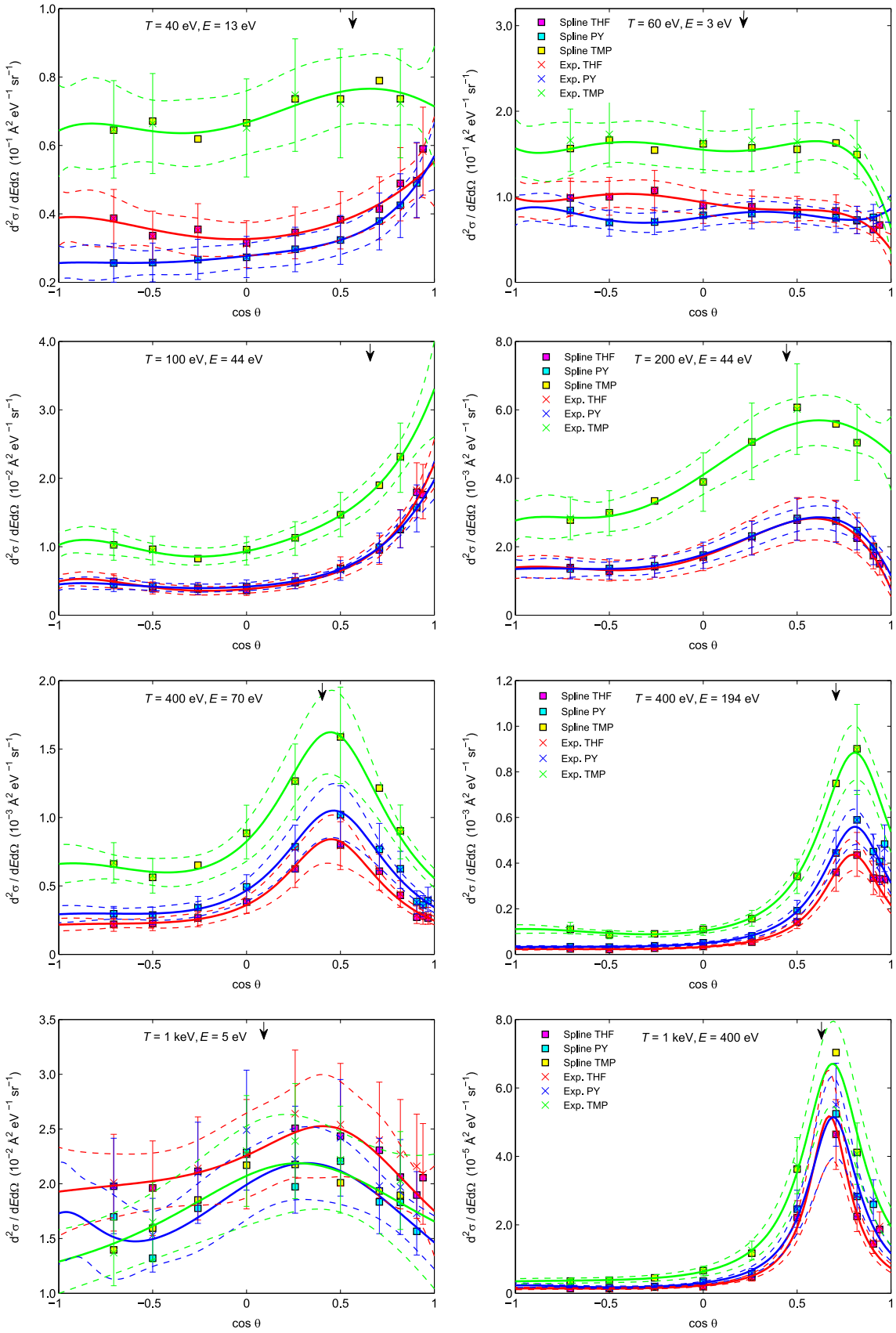

Fig. 9. DDCS of THF, PY and TMP for primary electrons of energy T and secondary electron energy E. Experimental data are shown as well as those obtained from the spline fit and the model functions (solid lines). Dashed lines are the uncertainties of the model functions. The arrow indicates the emission angle obtained from a kinematic model (Grosswendt and Waibel, 1978) (see text).

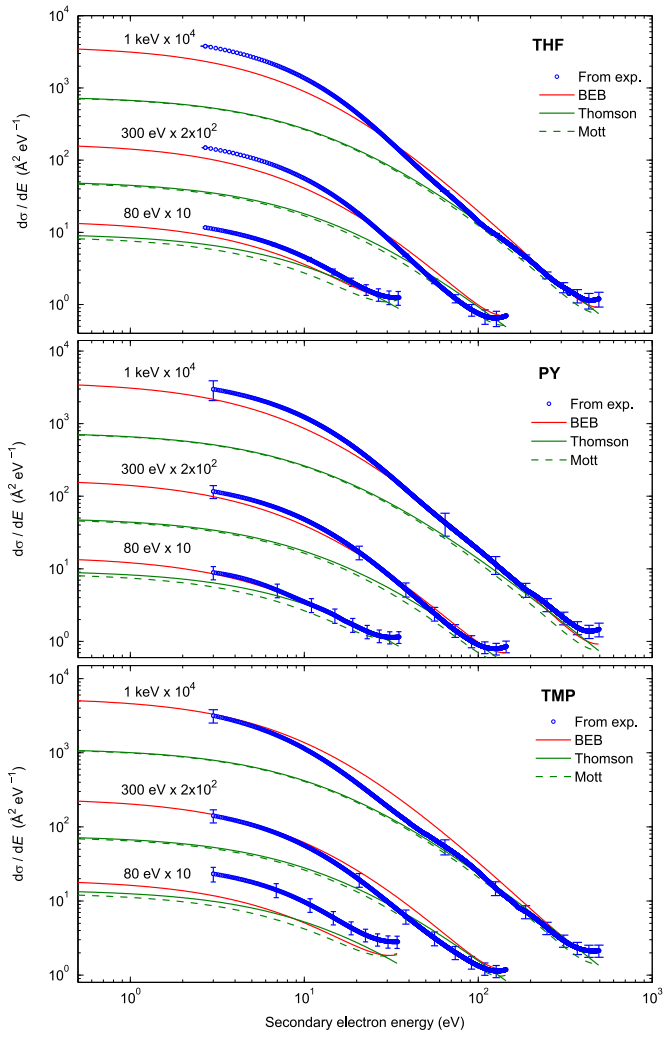

Fig. 10. SDCS of THF, PY and TMP obtained from the experimental data, the Thomson and Mott cross sections as well as the BEB model for primary electrons of selected energies. Uncertainties of data derived from the experiment are shown for selected data points to keep readability.

$$\frac{d\sigma_{ion}}{dE}(T > 25\ \text{eV}) = \frac{S'}{B'(t' + u' + 1)} \sum_{n=1}^{3} F_n[f_n(w') + f_n(t' - w')], \tag{10}$$

where

$$F_1 = -\frac{F_2}{t' + 1}, \quad F_2 = 2 - 1, \quad F_3 = Q' \ln t', \tag{11a}$$

$$f_n(w') = (w' + 1)^{-n}, \quad f_n(t' - w') = (t' - w')^{-n}, \tag{11b}$$

$$t' = T/B', \quad u' = U'/B', \quad w' = E/B' \tag{11c}$$

with fitting parameters S' (in units of Å^2), B' and U' (in units of eV) and Q'. Please note that this model function is applicable only for primary electron energies T between 25 eV and 1 keV. For lower primary electron energies, the SDCS can be assumed to be independent on the secondary electron energy (i.e. below 8 eV).

The parameters of Eq. (10) were themselves fitted as a function of the primary electron energies T (in eV). This was to achieve an interpolation of the SDCS with respect to the primary electron energy T as well as a convenient handling of the data for the implementation of the model in the simulation code. The following model functions were used

Table 4
Parameters for Eqs. (12a)–(12d).

THF							
q	200	ba_1	2.245×10^{1}	s_0	-1.069×10^{-2}	u_0	-1.463×10^{1}
		bb_1	1.368×10^{-1}	s_1	1.921×10^{-2}	u_1	-3.618×10^{-1}
		ba_2	-4.398×10^{2}	s_2	-1.686×10^{-3}	u_2	2.236×10^{-4}
		bb_2	2.870×10^{0}			u_3	-2.278×10^{-7}
PY							
q	200	ba_1	1.772×10^{1}	s_0	4.012×10^{-3}	u_0	-4.548×10^{0}
		bb_1	6.047×10^{-3}	s_1	1.170×10^{-2}	u_1	-3.054×10^{-1}
		ba_2	-1.088×10^{2}	s_2	-1.395×10^{-3}	u_2	3.872×10^{-4}
		bb_2	2.199×10^{0}			u_3	-2.258×10^{-7}
TMP							
q	200	ba_1	5.896×10^{1}	s_0	-8.507×10^{-2}	u_0	-1.006×10^{1}
		bb_1	4.216×10^{-1}	s_1	1.329×10^{-1}	u_1	-9.881×10^{-1}
		ba_2	-2.044×10^{2}	s_2	-6.452×10^{-2}	u_2	2.183×10^{-4}
		bb_2	1.575×10^{0}	s_3	1.028×10^{-2}		

$$Q' = q \tag{12a}$$

$$B' = \sum_{j=1}^{2} ba_j e^{-bb_j \log_{10} T} \tag{12b}$$

$$S'/B' = \sum_{j=0}^{s_{max}} s_j (\log_{10} T)^j \tag{12c}$$

$$U' = \sum_{j=0}^{u_{max}} u_j T^j \tag{12d}$$

The optimum fit parameters are given in Table 4. The parameters were fitted consecutively in the order above. This means that after the model function of one parameter was obtained, Eq. (10) was re-fitted to the SDCS data using only the remaining parameters. In this way, a good agreement with the SDCS data could be maintained.

The model functions of the SDCS are compared to the experimental data in Fig. 11. The uncertainties of experimental data are generally in the order of 25%.

At 30 eV impact energy, the model data of THF are in excellent agreement with experimental data while those of PY are up to 12% lower, which is well within experimental uncertainties. For TMP, the experimental data are overestimated by the model function by a factor of 1.5, which leads to large uncertainties of the model function values.

For primary electrons of energies T between 40 eV and 1 keV, the SDCS are in good agreement within the experimental uncertainties for secondary electron energies E below about 50 eV. Only at an energy T of 300 eV, the model function values are up to 27% larger than the experimental data. For secondary electron energies E above 50 eV, the model function generally underestimates the experimental data due to the choice of the BEB model for the fit. The magnitude of the deviations increases with increasing energy T and is a factor of two at 200 eV and a factor of five at 1 keV. However, in the energy regions of the observed deviations, the SDCS is two to three orders of magnitude smaller than for low secondary electron energies. In fact, the highest cross section is always present for energies E below 10 eV, where the model functions agree in most cases within 10% with the data derived from experiments for THF, PY and TMP.

When comparing the experimental SDCS data of THF, PY and TMP, normalized to the number of electrons (not shown), all SDCS agree within the uncertainties at primary electron energies T below 200 eV. At energies T above 200 eV, the agreement persists for secondary electron energies E above 20 eV, while the TMP data are up to 70% lower at an energy E of 3 eV. Such deviations are unexpected, as the production of low-energy electrons is well described within the first Born approximation and the respective cross sections scale approximately by the number of electrons in the target molecule. The observed deviations may arise from the different measurement technique applied

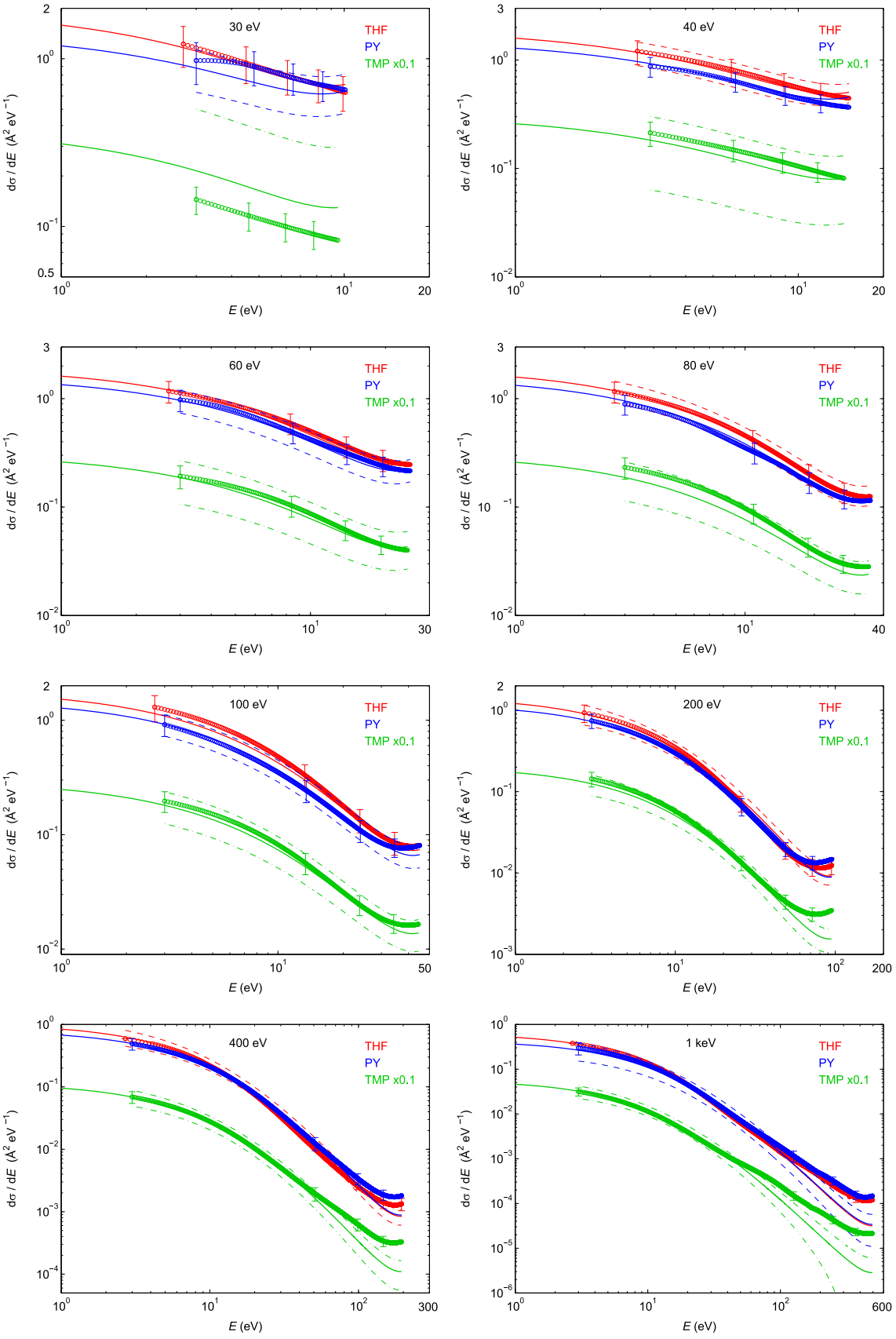

Fig. 11. SDCS of THF, PY and TMP for different primary electron energies, obtained from the experimental data by Eq. (6) (symbols) and the model function (lines). Uncertainties of the experimental data are shown for selected data points, while those of the model function are indicated by broken lines (for better readability, either the uncertainties of THF or PY are shown).

for TMP, namely the relative flow technique (Baek,), where nitrogen data were used to put the measured values to the absolute scale.

4.2.2.2. Purine. In accordance with the determination of the DDCS of PU, the SDCS of PY were scaled by the ratio of the respective total scattering cross sections.

4.3. Total ionization CS

The total ionization cross sections σ_{ion} were obtained by integrating the SDCS model functions by

$$\sigma_{ion}(T) = \int_{E_{min}}^{(T-B_0)/2} \frac{d\sigma}{dE} dE, \quad (13)$$

where B_0 is the energy of an outermost valence electron. The SDCS were previously obtained from the model functions provided in Eq. (10).

A delicate issue is the extrapolation of the SDCS towards zero electron energy. Due to the much larger values of the SDCS for low energies E, this extrapolation significantly increases the total ionization cross section. We show a comparison of data integrated with both lower energy limits, E_{min} (of 2.7 eV for THF and 3.0 eV for PY and TMP) used in the experiments and $E_{min} = 0$ eV, in Fig. 12. In fact, the total ionization cross section for electrons of energies T above 40 eV is larger than the integral starting at the experimental E_{min} by 20–40%. At 20 eV and 30 eV, the deviation is up to a factor of 2.5. This means that the extrapolation of the SDCS has to be carefully estimated.

4.3.1. Comparison to literature data

4.3.1.1. Tetrahydrofuran. The TICS obtained by integration from $E = 0$ eV of measured DDCS in this work (Fig. 12) are generally about 15% higher than those of Fuss et al. (2009), which were determined by measuring ionic fragments of THF produced by the impact of electrons of energies between 50 eV and 5 keV using time-of-flight spectrometry. The data of Fuss et al. are supported by the calculated values of Możejko and Sanche (2005) (12 eV–4 keV), deploying the BEB model also with an ionization threshold determined from experiments.

Theoretical TICS were also calculated by Limbachiya et al. (2015), using the spherical complex optical potential (SCOP) formalism to obtain inelastic cross sections and the complex scattering potential-ionization contribution method to determine the ionization component. Up to 200 eV, their TICS are up to 50% lower than those of Możejko and Sanche but still in good agreement with the experimental data of Fuss et al. Above 200 eV, the TICS of Limbachiya et al. are in excellent agreement with the TICS in our work and again reproduce the data of Fuss et al. at energies above 3 keV.

In contrast, the ab-initio calculations of Champion (2013)] are in good agreement with our TICS at energies up to 60 eV but rapidly drop at higher energies and continue about 60% lower than TICS of Fuss et al. or Możejko and Sanche. Moreover, the maximum is shifted to 60 eV, while the maxima of the other theoretical data, ours and those of Fuss et al. are at about 85 eV.

The position of the maximum in the data of Champion, however, is supported by the TICS measured by Dampc et al. (2011) using mass spectrometry for electron impact up to an energy of 150 eV to determine relative cross section data. In Fig. 12, these data were normalized at their maximum to the maximum value of Champion (2013) as in this way their data visually fit best among those of the other authors. Normalized in this way, the TICS of Dampc et al. support our TICS and those of Champion up to an energy of 60 eV. In comparison to the data of Fuss et al. and Możejko and Sanche, the data of Dampc et al. increase faster with increasing energy from the ionization threshold to the energy of the maximum. For energies between 60 eV and 150 eV, however, the data of Dampc et al. show a different behaviour than those of all other authors due to a less steeper slope.

In summary, published TICS of THF are diverse on the absolute scale and even more with respect to their energy dependence. For the evaluation of the model function (see below), we recommend to use our integrated values at energies up to 100 eV as these are in good agreement with the data of Dampc et al. (even if normalized to the maximum of the data of Fuss et al.) and Champion, and to rely rather on the TICS of Fuss et al. at higher energies as they are better supported by the theories.

4.3.1.2. Pyrimidine. TICS of PY in the literature can be divided into two groups with respect to the energy dependence (see Fig. 13). The TICS of the first group (Wolff et al., 2014; Champion et al., 2015) has a maximum at about 60 eV and rapidly drops at intermediate energies, while the TICS of the second group (Linert et al., 2012; Gupta et al., 2014) form a much broader maximum centered around 80 eV. Within the first group, Wolff et al. (2014) determined absolute TICS by the measurement of ionic fragments after electron impact (70–400 eV) using time of flight mass spectrometry. Their experimental data are well described over the entire energy range by the ab initio calculations of Champion et al. (2015) using a first Born approximation Coulomb wave approach. Wolff et al. provide also TICS from semi-empirical calculations, deploying a self-made model (Wolff et al., 2014), which show a similar energy dependence but are about 20% higher.

Within the second group, the TICS measured by Linert et al. (2012) (up to 150 eV) on the absolute scale by a total ion collection technique are in excellent agreement with the SCOP calculations of Gupta et al. (2014). However, in the region of the maximum (i.e. between 30 eV and 100 eV), the TICS of both groups are up to 45% lower than the TICS of all other authors. At energies higher than 200–300 eV, however, the data of Gupta et al. are larger than those calculated by Wolff et al. and Champion et al. (a factor of 1.7 at 1 keV). Remarkably, the TICS obtained in our work with a lower integration limit of $E = 3$ eV are in good agreement with the TICS of Linert et al. and Gupta et al.

The TICS obtained in our work with a lower integration limit of 0 eV are in excellent agreement with those of the first group (Wolff et al., 2014; Champion et al., 2015) up to an energy of about 70 eV but the energy of the maximum is at 80 eV, i.e. the maximum of the second group's TICS (Linert et al., 2012; Gupta et al., 2014). At energies above 100 eV, our TICS are a factor of 1.4 higher than those obtained by Wolff et al. experimentally, while at energies higher than 600 eV

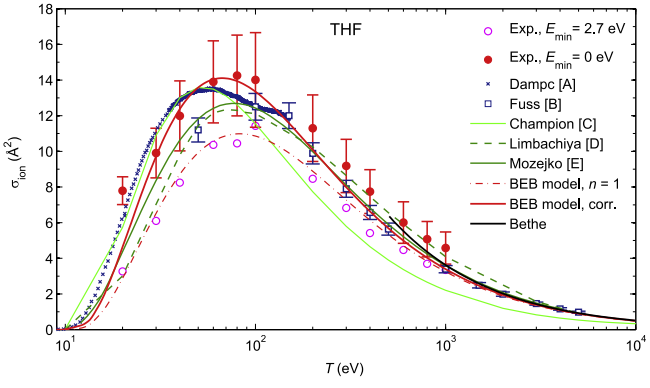

Fig. 12. Total ionization cross sections of THF obtained by integrating the measured DDCS data and calculated from the BEB model and the Bethe approximation. These are compared with literature data ((A) Dampc et al., 2011, (B) Fuss et al., 2009, (C) Champion, 2013, (D) Limbachiya et al., 2015, (E) Możejko and Sanche, 2005).

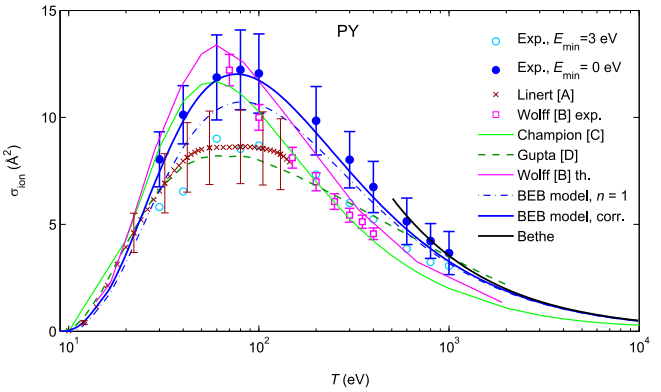

Fig. 13. Total ionization cross sections of PY obtained by integrating the measured DDCS data and calculated from the BEB model and the Bethe approximation. These are compared with literature data (A Linert et al., 2012, B Wolff et al., 2014, C Champion et al., 2015, D Gupta et al., 2014).

excellent agreement with the SCOP data of Gupta et al. is obtained.

As PY is a precursor of the pyrimidine nucleobases cytosine and thymine (as well as of uracil), the TICS of PY are also compared with the ionization cross sections of these molecules. Shafranyosh et al. (2006) determined TICS of cytosine from measuring the absolute yield of positive ions by a mass spectrometry technique. The energy dependence of their data is similar to the cross sections measured by Linert et al. (2012) for PY within the experimental uncertainties, while the absolute maximum value stated in their publication is about 11% lower.

TICS for cytosine and thymine have been calculated by several groups. For comparison in Fig. 14, the cross sections were normalized to the number of electrons in the respective molecule. Bernhardt and Paretzke (2003) used the Deutsch-Märk formalism as well as the BEB model with orbital electron energies obtained from restricted Hartree-Fock (RHF) calculations. The agreement between both models is reasonable in the region of the maximum but the deviation between the models increases with increasing energies, reaching 30% higher values for the BEB model at 1 keV (see Bernhardt and Paretzke, 2003). Fig. 14 shows the TICS obtained with the BEB model. Możejko and Sanche (2003) also used the BEB formalism to determine total ionization cross sections of the nucleobases. Fig. 14 shows that the normalized cross sections are up to 14% higher in the region of the maximum and about 10% higher at 1 keV than those of Bernhardt and Paretzke obtained with the BEB formalism. The TICS calculated by Możejko and Sanche are in excellent agreement with our data for PY within the uncertainties, while those of Bernhardt and Paretzke are comparatively lower. A third set of calculated cross sections is provided by Tan et al. (2004) (not shown to improve readability). These authors calculated inelastic cross sections by applying the dielectric response theory and the first Born approximation. For energies above 100 eV, their inelastic cross sections (being the sum of ionization and excitation cross sections) agree within 5% with the ionization cross sections determined by Możejko and Sanche (2003). Another data set for DNA nucleobases was calculated by Champion (2013) using the first Born approximation with a Coulomb wave description of the outgoing electron (not shown to improve readability). The TICS of Champion are significantly lower than those obtained by the other authors with the maximum being shifted to lower energies (consistent with the previous observation of Champion's data with respect to THF and PY).

4.3.1.3. Purine. Electron-impact ionization cross sections of PU were determined by integrating the respective SDCS, using $E_{min} = 0$ eV. Those data, divided by the number of electrons in the PU molecule, are shown in Fig. 14.

The literature data for adenine and guanine, calculated by the same authors as for the pyrimidine nucleobases (Bernhardt and Paretzke, 2003; Możejko and Sanche, 2003; Tan et al., 2004) show also similar discrepancies. The agreement between the TICS calculated by Możejko and Sanche (2003) and the total inelastics cross sections determined by Tan et al. (2004) is within 5%, while the data of Bernhardt and Paretzke (2003) are up to 22% and 15% higher than those of Możejko and Sanche in the maximum region and at 1 keV, respectively. The TICS calculated by Champion (2013) show the same behaviour as those for the PY nucleobases.

As for PY, the PU model function is best reproduced by the data of Możejko and Sanche (2003) in the region of the maximum, however, better agreement with the data of Bernhardt and Paretzke (2003) is observed at 1 keV.

4.3.1.4. Trimethylphosphate. In Fig. 15, TICS of TMP are compared to data calculated by Domaracka et al. (2007) for trimethylphosphine $P(CH_3)_3$ by means of the BEB model. In the graph, the latter data are multiplied by the ratio of the electron numbers of both molecules to enable comparison. In this case, the calculated data of both molecules agree within 10%. This agreement supports the previous suggestion that the values of TMP data for energies 300–1000 eV may be underestimated in the experiment (i.e. contrary to the absolute DDCS of THF and PY, the DDCS of TMP were measured only relative). The large uncertainty of the data point at 30 eV is due to the overestimation of the SDCS data by the SDCS model function.

4.3.2. TICS model function

In this work, the BEB model given in Eq. (14) was used to fit the total ionization cross section. This model also enables the calculation of partial ionization cross sections for each molecular subshell, which is required for the determination of the energy loss experienced by the scattered electron in track structure calculations.

The total ionization cross section is then

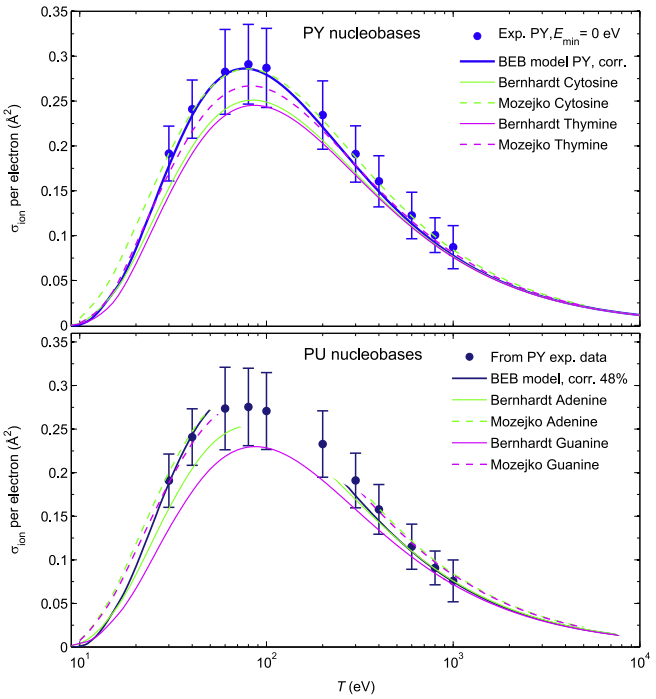

Fig. 14. Total ionization cross section of PY, cytosine and thymine (top) and of PU, adenine and guanine (bottom), divided by the respective number of electrons in the molecule. The PY data are compared to those for adenine and guanine calculated by Bernhardt and Paretzke (2003) and Możejko and Sanche (2003).

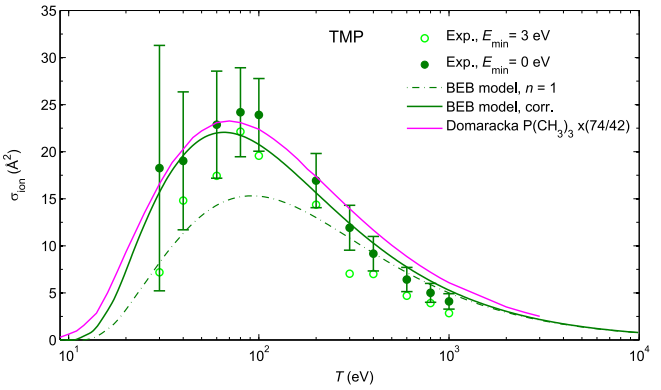

Fig. 15. Total ionization cross sections of TMP obtained by integrating the measured DDCS data and calculated from the BEB model compared to literature data (A Domaracka et al., 2007).

$$\sigma_{\mathrm{ion}}(T) = \sum_i \frac{S_i}{t + (u+1)/n_{\mathrm{BEB}}}\left[0.5\cdot Q\left(1 - \frac{1}{t^2}\right)\ln t + (2 - Q)\left(1 - \frac{1}{t} - \frac{\ln t}{t+1}\right)\right] \quad (14)$$

with $t = T/B_i$, $u = U_i/B_i$, $w = E/B_i$, Q=1, $S_i = 4\pi a_0^2 N_i (R/B_i)^2$, R is the Rydberg constant, a_0 is the Bohr radius and N_i is the number of electrons in the i-th subshell. Parameters B_i and U_i, the binding and kinetic energies of electrons occupying this subshell, are given in Table 6. In addition, the parameter n_{BEB} was introduced in the BEB model as suggested by Irikura et al. (2003). This parameter was essentially used as a fit parameter. It was determined on the basis of a Mulliken population analysis performed with GAMESS (Gordon research group,) for the molecules investigated in this work. Irikura et al. used this empirical parameter to reduce the contribution of the average kinetic energy of electrons in a molecular orbital, which can be predominantly allocated to atomic orbitals with principal quantum numbers larger than two (Irikura et al. proposed a parameter n_{BEB} equal to the principal quantum number of the respective atomic orbital in which the Mulliken population is >0.5). The best agreement with the data derived from the experiment is obtained for Mulliken populations larger than 0.40 for THF, 0.47 for PY, 0.48 for PU and 0.34 for TMP. The factors n_{BEB} are listed in Table 5 for each molecular subshell.

The original version of the BEB model (using $n_{\mathrm{BEB}} = 1$) with energy parameters from Table 6 dramatically underestimates the integrated experimental data at energies below about 300 eV, when an extrapolation to zero secondary electron energy is applied. This is in accordance with the underestimation of the SDCS for the production of low energy secondary electrons. It is worthwhile to notice that the ionization threshold has a significant impact on the calculated total ionization cross section. Using the experimental values of the ionization threshold (as given in Table 6), the total ionization cross sections increased by 8–10% at 20 eV.

The description of the integrated experimental data (from 0 eV) is significantly improved by using the parameters n_{BEB} as listed in Table 5 in the BEB model (Figs. 12, 13, 15).

For THF, integrated experimental data agree with the BEB model within the uncertainties except for the data points at 20 eV and 1 keV. In particular, the model function is in agreement with our recommendations above, i.e. excellent agreement with our data, those of Dampc et al. (2011) and Champion (2013) is observed for energies up to 100 eV, whereas for energies above, the model function reproduces the TICS of Fuss et al. (2009) and Możejko and Sanche (2005).

For PY, the model function data agree well with our integrated experimental values. The shape of the maximum TICS at 70–100 eV is supported by the data of Linert et al. (2012) and Gupta et al. (2014), outlining that both data sets are in excellent agreement with our TICS when the integration is performed from E=3 eV. For this reason, we see our data at higher energies supported by the calculations of Gupta et al. (2014). Furthermore, the good agreement with the TICS of THF at higher energies affirms the consistency of both data sets. The absolute maximum value of our TICS finds support in the TICS of Wolff et al. (2014) and Champion et al. (2015). In addition, the model function is supported by BEB calculations for cytosine and thymine (Bernhardt and Paretzke, 2003; Możejko and Sanche, 2003).

For PU, the model function is in excellent agreement with the TICS derived from those of PY and the BEB calculations for adenine and guanine (Bernhardt and Paretzke, 2003; Możejko and Sanche, 2003).

For TMP the situation is less satisfying. For energies up to 400 eV, the model function describes the integrated experimental data within the uncertainties. However, we point out that the data point at 30 eV is 16% larger than the model data and has a very large uncertainty, which is both due to the overestimation of the SDCS data by the SDCS model function. On the other hand, the data points at energies 80, 100 and 200 eV are 10% larger, despite the lower SDCS model data compared to the experimental SDCS values. The deviations of the SDCS model data essentially arise from the fit of the SDCS model function parameters as a function of energy T. Nonetheless, the resulting larger uncertainties of the total ionization cross section data are acceptable, as the absolute values obtained by this procedure are more realistic. At energies 600–1000 eV, the model function of the total ionization cross section is as much as 25% higher than the integrated data. This deviation is not due to the underestimation of the SDCS at high energies E by the SDCS model function, as this affects the total ionization cross section by less than 6%. Rather, as stated before, the observed deviations in the total and differential TMP data may arise from the data analysis of the data measured by the relative flow technique and put to the absolute scale by using nitrogen data (Baek,). The model function agrees within 10% with the TICS calculated by Domaracka et al. (2007) for trimethylphosphine, scaled to the number of valence electrons of TMP.

4.3.2.1. Bethe approximation. In the high energy range, the cross section data are compared to the Bethe approximation. Kim et al. (2000) suggested expressions for the constants derived from the BEB model, which are needed in the relativistic version of the Bethe cross section

$$\sigma_{\mathrm{Bethe}} = \frac{4\pi a_0^2 \alpha^2}{\beta_t^2}\sum_{i=1}^{i_{\max}} M_i^2\left[\ln\left(\frac{\beta_t^2}{1-\beta_t^2}\right) - \beta_t^2 + C_{Ri}\right], \quad (15)$$

Table 5
Factors n_{BEB} applied to the BEB model for the calculation of the total ionization cross sections of THF, PY, PU and TMP listed for each molecular subshell.

	THF	PY	PU	TMP		THF	PY	PU	TMP
1	1	1	1	1	20	1	1	3	1
2	1	1	1	1	21		1	1	3
3	1	1	1	1	22			3	3
4	1	1	1	1	23			3	3
5	1	1	1	1	24			1	3
6	3	1	1	1	25			1	3
7	3	3	1	1	26			1	3
8	3	3	1	1	27			1	3
9	3	3	1	3	28			3	3
10	3	3	3	1	29			3	3
11	1	3	3	1	30			1	3
12	3	1	3	1	31			1	3
13	1	3	3	3	32				3
14	3	1	3	3	33				3
15	3	3	3	3	34				3
16	3	1	3	1	35				3
17	3	1	3	1	36				3
18	1	1	3	1	37				3
19	3	1	3	1					

Table 6
Binding energies B_i and kinetic energies U_i of electrons in the i-th subshell of THF, TMP, PY and PU.

i	THF		TMP		PY		PU	
	B_i (eV)	U_i (eV)	B_i (eV)	U_i (eV)	B_i (eV)	U_i (eV)	B_i (eV)	U_i (eV)
1	557.94	792.08	2178.05	2884.91	423.44	600.34	424.98	600.10
2	306.17	434.60	559.41	792.92	423.44	600.26	423.64	600.28
3	306.17	434.55	559.40	792.92	307.52	434.52	423.43	600.33
4	305.08	434.55	559.40	792.92	307.09	434.53	423.31	600.29
5	305.07	434.50	557.34	793.18	307.09	434.56	308.17	434.53
6	36.97	64.50	306.92	435.01	305.92	434.53	308.14	434.49
7	28.97	41.98	306.92	435.01	36.57	49.14	307.64	434.53
8	27.21	40.28	306.92	435.00	33.02	56.54	307.19	434.54
9	22.25	41.00	209.59	431.58	29.75	46.27	306.53	434.48
10	22.14	37.51	152.44	401.58	24.64	45.73	38.22	48.15
11	18.69	28.34	152.42	401.50	24.55	45.85	36.26	50.28
12	18.19	32.70	152.42	401.50	20.52	29.17	33.67	55.49
13	16.28	27.08	39.64	68.08	19.37	45.44	32.44	57.92
14	15.97	37.84	37.67	72.85	17.98	34.88	29.34	49.57
15	15.11	42.95	37.67	72.85	16.53	37.22	25.41	45.45
16	13.60	38.10	35.23	76.82	16.27	40.42	24.35	48.62
17	13.57	35.51	27.43	46.58	15.96	29.49	23.52	44.56
18	12.99	30.83	26.20	44.06	12.58	50.73	21.70	40.36
19	12.31	53.44	26.20	44.06	11.54	36.60	20.09	40.14
20	9.74[a]	55.63	21.40	56.86	10.96	51.35	19.11	46.88
21			19.37	47.92	9.73[b]	31.00	17.90	43.80
22			19.37	47.92			17.88	30.70
23			18.44	44.65			17.18	42.92
24			17.85	36.99			16.56	39.21
25			17.85	36.99			15.05	33.83
26			17.13	36.25			13.44	52.33
27			17.09	42.62			12.92	36.81
28			17.09	42.62			12.22	52.04
29			15.90	50.66			10.97	52.39
30			14.33	49.71			10.57	42.28
31			14.33	49.71			9.58	35.13
32			13.59	56.69				
33			13.32	53.35				
34			13.32	53.35				
35			12.90	61.39				
36			10.81[c]	60.91				
37			10.81[c]	60.91				

[a] Measured value (NIST, 2013).
[b] Measured value (Hush and Cheung, 1975).
[c] Measured value (Tasaki et al., 1990).

where $\beta_t^2 = 1 - 1/(1 + T/mc^2)^2$, $C_{Ri} = \ln(R/B_i) + 2M_i^2(1 - \ln\alpha)$, α is the fine structure constant, mc^2 is the rest energy of an electron and the other symbols are described above (see Eq. (7)). Due to the absence of data for differential oscillator strengths, required for an accurate calculation of the Bethe cross section, the above formula was used. Ionization cross sections obtained by Eq. (15) are also shown in Figs. 12, 13 and 15 to reproduce the BEB cross section data at energies above 1 keV.

4.3.3. Fano plot

A Fano plot is used in Fig. 16 to investigate the consistency of the total ionization cross sections. In the high energy range, a linear dependence of the normalized cross section data on $\ln(T/R)$ should occur. This is the case for the BEB model functions of THF and PY in this work, which have a slightly lower slope than the data of Możejko and Sanche (2005). The data of Fuss et al. (2009) show the largest slope.

A comparison of the Bethe cross section of THF reveals that the slope of those data is in agreement with the slope in the data of Możejko but of lower magnitude on the y-axis (the data of Możejko are about 4% higher than the Bethe cross section). The BEB model data in our work were calculated with the nonrelativistic version and tend to have a decreasing slope towards higher energies. However, the relativistic version of the BEB model (not shown to keep readability) shows also good agreement with the slope of the Bethe model. In the case of TMP, the kink at 300 eV in the Fano plot supports the assumption made above, that the total ionization cross sections derived from the experimental data are too low and the model function is a more realistic description. Nonetheless, a recalculation of the Bethe cross section, directly using oscillator strength data, would be necessary to further investigate the consistency of our data.

In summary, the BEB model function values for THF, PY and TMP are in agreement with literature data as well as with the Bethe cross section at high energies.

5. Excitation cross sections

Total excitation cross sections were calculated by subtracting the total cross sections for ionization $\sigma_{ion}(T)$ and elastic scattering $\sigma_{el}(T)$ from the total scattering cross sections $\sigma_t(T)$, such that

$$\sigma_{exc}(T) = \sigma_t(T) - \sigma_{ion}(T) - \sigma_{el}(T). \quad (16)$$

The complete set of total scattering cross sections of DNA constituents is shown in Fig. 17. Excitation cross sections, determined from Eq. (16), generally decrease with increasing electron energy after a maximum just below 10 eV. However, these data show an unexpected dip around 100 eV, the origin of which still has to be investigated. In fact, the excitation cross section is more than one order of magnitude lower than the other total cross sections in this energy region and therefore very sensitive to their variations. Several sources for this dip are possible. For example, an underestimation of the TCS in this energy range (at 100 eV, a higher TCS by 17% would lead to excellent agreement with the data of Fuss et al., 2014) appears likely due to the incomplete contribution of electrons scattered by rotational excitation in the measurement. Another reason could be an overestimation of the extrapolated SDCS at low secondary electron energies, which would have a considerable influence on the TICS. Finally, an overestimation of the TelCS by the extrapolation procedure cannot be excluded.

5.1. Tetrahydrofuran

To this date, several excitation cross sections for low-energy electrons have been published (Allan, 2007; Dampc et al., 2007b; Bouchiha et al., 2006; Do et al., 2011; Khakoo et al., 2013, 2015) (see Fig. 18).

Cross sections for electronic excitation states, however, were measurement Do et al. (2011) who determined differential electron-impact cross sections (15–50 eV, 15–90°) of the three lowest lying Rydberg bands in THF, with vertical excitation energies of 6.6, 7.2 and 7.8 eV. The differential data were extrapolated with respect to the scattering angles by molecular phase shift analysis (Do et al., 2011) and integral cross sections are provided. The sum of their integral excita-

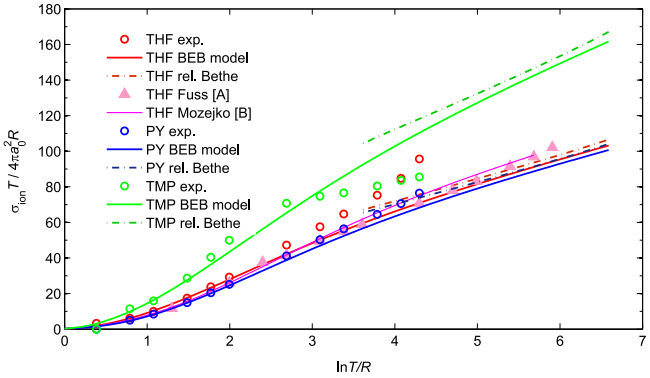

Fig. 16. Fano plot of the total ionization cross sections of THF, PY and TMP compared to literature data ([A] Fuss et al., 2009, [B] Możejko and Sanche, 2005).

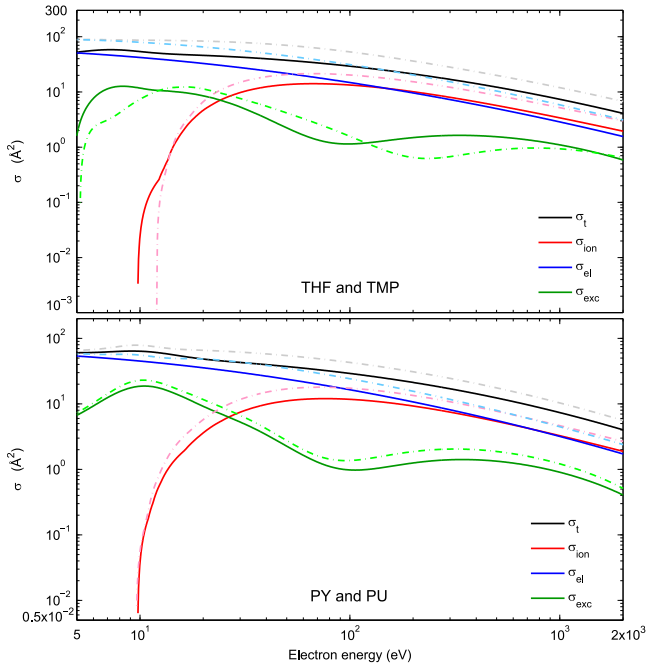

Fig. 17. Total scattering cross sections σ_t and total cross sections for scattering of electrons on THF, PY (solid lines), TMP and PU (broken lines), leading to ionization σ_{ion}, elastic scattering σ_{el} and excitation σ_{exc}, respectively.

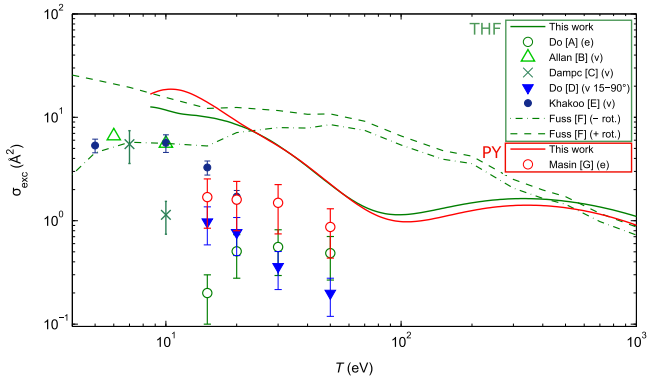

Fig. 18. Total excitation cross sections of THF and PY. Literature data on vibrational (v) and electronic (e) excitation cross sections are also shown (A Do et al., 2011, B Allan, 2007, C Dampc et al., 2007b, D Do et al., 2015, E Khakoo et al., 2013, G Mašín et al., 2012) as well as the total excitation cross section of Fuss et al. (F) Fuss et al., 2014.

tion cross sections for the three lowest Rydberg states is shown in Fig. 18. Three additional Rydberg states are present with vertical excitation energies of 8.1, 8.57 and 8.89 eV (Bremner et al., 1991; Bouchiha et al., 2006) so that the data of Do et al. are lower than the total electronic excitation cross sections.

Vibrational excitation cross sections of THF have been measured differentially as function of scattering angle by Allan (2007) (up to 16 eV, 45–180°), Dampc et al. (2007b) (4.5–14 eV, 20–180°), Khakoo et al. (2013) (2–15 eV, 15–130°) and Do et al. (2015) (15–50 eV, 15–90°) with electron energy loss spectroscopy. Allan provides absolute values, while the other authors normalized their measured data to elastic scattering cross sections of different groups. Integral values are given by Allan (for 6 eV and 10 eV) and by Khakoo et al. as the sum over all vibrational modes, while Dampc et al. provide the integral only for the most pronounced energy loss peak describing the CH2 stretch mode around 350 meV for 7 eV and 10 eV electron impact as well as the integral of the CC stretch mode around 140 meV energy loss for 7 eV. In Fig. 18, the sum over both vibrational excitation modes is shown for 7 eV. Generally, the sum of integral vibrational excitation cross sections of Allan, Khakoo et al. and Dampc et al. (only the 7 eV data point) are in excellent agreement.

The vibrational excitation cross sections measured by Do et al. (2015) were integrated over the scattering angles of the experiment (15–90°) and are also shown in Fig. 18. Due to the incomplete integration, the integral values are lower, but on the same order of magnitude as those of the other authors.

Another set of excitation cross sections is provided by Fuss et al. (2014). These data were derived on the basis of measured total scattering and total ionization cross sections and using theoretical calculations to determine elastic scattering and rotational excitation cross sections in thorough comparison to available literature data. Their total excitation cross sections shown in Fig. 18 contain the contribution of vibrational excitations, electronic excitation, those leading to neutral dissociation and are plotted either with or without including rotational excitations. The total excitation cross section in this work is on the same order of magnitude as the values proposed by Fuss et al. (2014), but differences of up to a factor of five at 100 eV are present.

At energies below 20 eV it is obvious that the excitation cross section in our work contains a contribution by rotational excitations. For energies above 20 eV, this contribution is to a larger extent contained in the elastic scattering cross section, as the DelCS were measured for scattering angles of 5°, while those for energies below 20 eV were measured from 20°.

A mean excitation energy of 8.01 eV was obtained for THF from optical oscillator strength distributions provided in the detailed study of Giuliani et al. (2008), where absolute photoabsorption cross sections were determined from measurements between 5.8 and 10.6 eV and supported by ab-initio calculations. Their results are also in good agreement with the vacuum ultraviolet absorption spectra and electron energy loss spectra of Bremner et al. (1991) as well as with quantum-mechanical R-matrix calculations of the resonance peaks by Bouchiha et al. (2006).

It is interesting to note that the two conformations with C_2 and C_s symmetry in which the THF molecules coexist have a significant impact on excitation energies and oscillator strengths (Giuliani et al., 2008; Bouchiha et al., 2006). However, the mean value of the excitation energy is not significantly different for both conformers when calculated from the sum of excitation energies weighted by the oscillator strengths given by Giuliani et al. (2008). In this case, mean excitation energies for dipole-allowed transitions were 7.95 eV and 8.07 eV for the C_s and C_2 geometries, respectively. The average value of 8.01 eV was applied in the simulations to determine the energy loss in an excitation process.

5.2. Pyrimidine

Electronic and vibrational excitation of PY has been investigated, for example, by Ferreira da Silva et al. (2010), Jones et al. (2012) and Mašín et al. (2012). Ferreira da Silva et al. (2010) used vacuum ultraviolet absorption spectroscopy in the energy range 3.7–10.8 eV and electron energy loss spectroscopy between 2 eV and 15 eV and thoroughly compared their results to previous data. The vertical excitation energies of these authors agree well with those measured by Mašín et al. (2012) by electron energy loss spectroscopy for the impact of electrons of energies 15–50 eV. The theoretical R-matrix calculations at 15 eV also published by Mašín et al. support their experimental data. This group (Jones et al., 2012; Mašín et al., 2012) derived integral electron-impact cross sections for electronic excitations from their measurement of differential electron energy loss spectra based on the known properties of the generalized oscillator strength for dipole allowed transitions (Mašín et al., 2012). In Fig. 18, the total excitation cross section calculated in this work is higher than the sum of the integral electronic excitation cross sections of Mašín et al. The difference might be filled by the contribution of vibrational

excitation cross sections, which is however unknown to this date.

Mašín et al. (2012) separately provided cross section values for 7 electronic levels. Based on their data, the average energy loss was determined as function of incident electron energy. For electrons of 15, 20, 30 and 50 eV the average energy loss is 6.92, 7.34, 7.56 and 7.59 eV, respectively. As expected, those values show asymptotic behaviour towards high electron energies. To verify the asymptotic value, the mean excitation energy was calculated similarly to the value for THF, i.e. using the oscillator strength distribution of Stener et al. (2011). Only electronic transitions with transition energies below the ionization threshold of 9.7 eV were considered to compare the value to the data of Mašin et al. (however, it should be kept in mind that intravalence transitions to excitation levels above the ionization threshold have significant oscillator strengths). The mean excitation energy for dipole-allowed transitions with excitation energies below the ionization threshold is 7.61 eV which is consistent with the asymptotic average excitation energy of Mašin et al.

Generally, the scattering angle of the electron after an electronic excitation is strongly directed in forward direction as shown by Jones et al. (2012). Hence, in the simulations a 0° scattering angle is applied.

As long as there exist no cross section data for the excitation to specific states of THF and for the excitation of PY by electrons of energies below 15 eV, simulations may be performed using the mean excitation energy of 7.61 eV in the dipole-limit and forward scattering. The potential error introduced by these assumptions in the simulation results appears acceptable.

5.3. Trimethylphosphate and purine

Unfortunately, no literature data on excitation cross section data or oscillator strength distributions exist for TMP and PU. Due to the similarity in molecular structure of PY and PU, an excitation energy of 7.61 eV is also used for PU. In the case of TMP, the same excitation energy of THF of 8.01 eV was used as the bond structure of valence orbitals in both molecules is similar.

6. Conclusions

Model functions for calculating a cross section data set for electron-impact on tetrahydrofuran, trimethylphosphate, pyrimidine and purine were developed based on a comprehensive set of experimental data and a literature review. This data set can be readily used for track structure simulations of electrons with energies between about 30 eV and 1 keV.

When using the data set at energies below 30 eV, it should be kept in mind that the presented data were measured for gas-phase DNA constituents. In the condensed phase, however, neighbouring molecules distort the local electron density distribution, resulting in changes of the scattering process and the interaction cross sections (Sanche, 2005). The scattering of electrons with energies below 30 eV is particularly affected as their wave length is in the order of the bond lengths within one molecule and the distance between molecules in the condensed phase.

In the condensed phase, generally, the screening of electron interactions by neighbouring molecules leads to a shift of oscillator strengths to higher energies (Inokuti, 1991) and, hence, to a reduction of electronic excitation cross sections. Furthermore, a decrease in the orbital ionization potentials is expected, which would increase the ionization cross section. However, this increase is, in part, compensated by intra- and inter-molecular incoherent and coherent scattering of ejected low-energy electrons (Inokuti, 1991). In addition, the screening effect reduces the polarisation of the molecular electron density distribution by a passing slow electron which further reduces the ionization probability (Inokuti, 1991). The lower polarisation effect also affects the elastic cross section by decreasing the probability for forward scattering and, hence, also the total elastic cross section. Furthermore, coherent multiple scattering may span not only across one molecule but over several molecules as the electron wavelength is in the same order of magnitude as inter- and intra-molecular dimensions. Additional channels, such as delocalised excitations spanning across a large number of molecules occur and contribute to the total cross section.

Due to the expected changes in cross section data if condensed phase DNA is modeled, we recommend the presented data for energies

Table 7
Total electron-impact cross sections of THF and TMP. Units are in Å^2.

T (eV)	THF				TMP			
	σ_t	σ_{ion}	σ_{el}	σ_{exc}	σ_t	σ_{ion}	σ_{el}	σ_{exc}
9	55.91 ± 0.54	0.00	43.48 ± 2.49	12.44	86.83	0.00	80.97 ± 51.79	5.86
10	53.85 ± 0.48	0.02	42.07 ± 2.31	11.75	86.63	0.00	79.16 ± 45.75	7.47
15	48.00 ± 0.62	1.34	36.62 ± 1.74	10.04	85.22	2.22	71.33 ± 26.92	11.67
20	45.92 ± 0.63	4.64 ± 3.51	32.79 ± 1.48	8.49 ± 6.42	83.29	7.35	65.18 ± 17.62	10.75
25	44.23 ± 0.59	7.55 ± 2.06	29.89 ± 1.33	6.79 ± 1.88	81.12	12.26	60.24 ± 12.57	8.63
30	42.66 ± 0.51	9.72 ± 2.29	27.60 ± 1.24	5.34 ± 1.28	78.85	15.69 ± 13.30	56.15 ± 9.74	7.01 ± 6.07
35	41.20 ± 0.48	11.29 ± 2.06	25.72 ± 1.17	4.19 ± 0.79	76.55	18.01 ± 10.53	52.70 ± 8.13	5.84 ± 3.53
40	39.84 ± 0.46	12.37 ± 2.29	24.14 ± 1.12	3.33 ± 0.64	74.27	19.58 ± 7.76	49.73 ± 7.22	4.95 ± 2.09
45	38.59 ± 0.46	13.11 ± 2.30	22.79 ± 1.07	2.70 ± 0.49	72.04	20.67 ± 7.47	47.15 ± 6.68	4.23 ± 1.64
50	37.44 ± 0.46	13.59 ± 2.30	21.62 ± 1.03	2.24 ± 0.39	69.89	21.36 ± 7.18	44.88 ± 6.34	3.66 ± 1.33
60	35.36 ± 0.45	14.04 ± 2.30	19.67 ± 0.96	1.66 ± 0.28	65.84	21.98 ± 6.59	41.04 ± 5.91	2.82 ± 0.94
70	33.56 ± 0.46	14.09 ± 2.29	18.10 ± 0.90	1.36 ± 0.23	62.15	22.01 ± 6.61	37.90 ± 5.59	2.24 ± 0.75
80	31.97 ± 0.46	13.94 ± 2.28	16.81 ± 0.84	1.21 ± 0.21	58.82	21.73 ± 6.64	35.28 ± 5.30	1.81 ± 0.62
90	30.55 ± 0.48	13.67 ± 2.51	15.73 ± 0.80	1.15 ± 0.22	55.82	21.28 ± 6.35	33.05 ± 5.02	1.49 ± 0.50
100	29.28 ± 0.49	13.35 ± 2.73	14.79 ± 0.76	1.14 ± 0.24	53.11	20.75 ± 6.06	31.12 ± 4.75	1.24 ± 0.41
150	24.46 ± 0.53	11.58 ± 2.45	11.56 ± 0.61	1.32 ± 0.29	42.91	17.96 ± 4.68	24.34 ± 3.57	0.61 ± 0.18
200	21.17 ± 0.56	10.09 ± 2.16	9.59 ± 0.51	1.49 ± 0.33	36.26	15.63 ± 3.30	20.17 ± 2.72	0.47 ± 0.12
250	18.76 ± 0.58	8.92 ± 2.03	8.25 ± 0.45	1.59 ± 0.37	31.59	13.81 ± 2.55	17.29 ± 2.13	0.48 ± 0.11
300	16.88 ± 0.59	7.99 ± 1.90	7.27 ± 0.40	1.63 ± 0.40	28.12	12.38 ± 1.80	15.18 ± 1.72	0.56 ± 0.10
400	14.15 ± 0.60	6.63 ± 1.61	5.90 ± 0.34	1.62 ± 0.41	23.25	10.28 ± 2.13	12.25 ± 1.25	0.71 ± 0.16
500	12.22 ± 0.59	5.69 ± 1.55	4.99 ± 0.31	1.54 ± 0.44	19.95	8.82 ± 1.99	10.30 ± 1.04	0.82 ± 0.20
600	10.78 ± 0.58	4.99 ± 1.49	4.33 ± 0.29	1.45 ± 0.45	17.53	7.75 ± 1.85	8.90 ± 0.96	0.89 ± 0.23
700	9.65 ± 0.56	4.45 ± 1.46	3.84 ± 0.27	1.36 ± 0.46	15.68	6.92 ± 1.71	7.84 ± 0.93	0.92 ± 0.25
800	8.74 ± 0.55	4.03 ± 1.42	3.44 ± 0.26	1.27 ± 0.46	14.20	6.26 ± 1.56	7.00 ± 0.92	0.93 ± 0.26
900	7.99 ± 0.54	3.68 ± 1.45	3.13 ± 0.25	1.18 ± 0.48	12.98	5.73 ± 1.50	6.33 ± 0.91	0.92 ± 0.28
1000	7.36 ± 0.52	3.39 ± 1.47	2.86 ± 0.24	1.10 ± 0.49	11.97	5.28 ± 1.45	5.78 ± 0.91	0.91 ± 0.29

Table 8
Total electron-impact cross sections of PY and PU. Units are in Å^2.

T (eV)	PY				PU			
	σ_t	σ_{ion}	σ_{el}	σ_{exc}	σ_t	σ_{ion}	σ_{el}	σ_{exc}
9	63.94 ± 1.92	0.00	46.42 ± 3.40	17.56	78.23	0.00	56.75	21.48
10	63.64 ± 1.99	0.04	45.02 ± 3.13	18.62	78.51	0.06	55.49	22.97
15	54.97 ± 2.04	1.51	39.50 ± 2.39	14.02	68.61	2.44	49.23	16.94
20	48.34 ± 2.00	3.60	35.56 ± 2.12	9.24	65.76	5.73	48.30	11.73
25	45.03 ± 2.02	5.71	32.55 ± 2.01	6.83	63.72	9.00	45.97	8.74
30	42.88 ± 2.01	7.46 ± 1.42	30.15 ± 1.95	5.34 ± 1.10	61.69	11.65	43.28	6.76
35	41.17 ± 2.00	8.80 ± 1.42	28.16 ± 1.90	4.27 ± 0.77	59.76	13.61	40.79	5.35
40	39.69 ± 1.99	9.83 ± 1.42	26.49 ± 1.86	3.43 ± 0.58	57.93	15.09	38.57	4.26
45	38.37 ± 2.00	10.58 ± 1.56	25.05 ± 1.82	2.80 ± 0.48	56.21	16.15	36.61	3.44
50	37.18 ± 2.00	11.11 ± 1.71	23.80 ± 1.77	2.32 ± 0.42	54.60	16.89	34.86	2.84
60	35.09 ± 2.02	11.74 ± 1.99	21.71 ± 1.69	1.70 ± 0.33	51.67	17.70	31.88	2.09
70	33.30 ± 2.03	11.99 ± 1.94	20.02 ± 1.61	1.36 ± 0.26	49.09	17.96	29.43	1.71
80	31.75 ± 2.03	12.01 ± 1.88	18.63 ± 1.54	1.17 ± 0.22	46.80	17.91	27.37	1.52
90	30.37 ± 2.03	11.91 ± 1.88	17.44 ± 1.47	1.08 ± 0.21	44.75	17.68	25.62	1.46
100	29.14 ± 2.03	11.73 ± 1.88	16.43 ± 1.41	1.04 ± 0.20	42.90	17.35	24.10	1.45
150	24.45 ± 2.01	10.48 ± 1.77	12.88 ± 1.16	1.14 ± 0.24	35.79	15.31	18.77	1.71
200	21.24 ± 1.99	9.28 ± 1.66	10.71 ± 0.99	1.30 ± 0.29	30.91	13.46	15.51	1.94
250	18.86 ± 1.99	8.29 ± 1.54	9.22 ± 0.88	1.40 ± 0.33	27.30	11.96	13.28	2.06
300	17.00 ± 1.99	7.48 ± 1.42	8.12 ± 0.80	1.45 ± 0.35	24.51	10.76	11.64	2.10
400	14.26 ± 2.01	6.27 ± 1.27	6.59 ± 0.70	1.44 ± 0.39	20.42	8.98	9.39	2.05
500	12.31 ± 2.02	5.41 ± 1.20	5.57 ± 0.64	1.37 ± 0.41	17.54	7.73	7.89	1.93
600	10.85 ± 2.03	4.76 ± 1.13	4.84 ± 0.60	1.28 ± 0.42	15.39	6.80	6.82	1.78
700	9.70 ± 2.03	4.26 ± 1.00	4.28 ± 0.57	1.19 ± 0.41	13.72	6.08	6.01	1.63
800	8.77 ± 2.02	3.87 ± 0.88	3.84 ± 0.55	1.09 ± 0.39	12.37	5.50	5.37	1.49
900	8.00 ± 2.01	3.54 ± 0.98	3.48 ± 0.54	1.01 ± 0.41	11.26	5.04	4.86	1.37
1000	7.36 ± 2.00	3.27 ± 1.07	3.19 ± 0.52	0.93 ± 0.42	10.33	4.65	4.44	1.25

above 30 eV, but to apply those below 30 eV with caution.

Values and uncertainties related to the model functions of the total cross section data are provided in Appendix B, while differential cross sections may be calculated using the provided model functions.

The data set has already been implemented in the track structure code PTra (Bug et al., 2014) and will also be available in Geant4-DNA (Incerti et al., 2010).

Acknowledgements

The authors thank Dr. Daniel Bennett for fruitful discussions. This work was carried out within the EMRP Joint Research Project BioQuaRT. The EMRP is jointly funded by the EMRP participating countries within EURAMET and the European Union.

Appendix A. Parameters for the BEB model

For the BEB model, the binding energies B_i and average kinetic energies U_i of electrons bound in the i-th molecular subshell are required. These parameters were obtained by means of GAMESS (Gordon research group, 2013), using the restricted Hartree-Fock (RHF) method and the 6–311G basis set. The results for THF, TMP, PY and PU are listed in Table 6. As orbital energies calculated by the RHF method are often higher than the vertical ionization energy (Bransden and Joachain, 1983), we followed the example of other authors and substituted the binding energies of the outermost valence electrons by experimental values of the ionization threshold. In the case of TMP, the binding energies of the four outermost electrons were adjusted due to the C_3 symmetry of the molecule.

The calculated binding energies of THF are generally larger (in their absolute values) than vertical ionization energies determined by photoelectron spectroscopy (Dampc et al., 2007b; Giuliani et al., 2008) and electron energy loss spectroscopy (Duflot et al., 2010). In fact, the overestimation is 0.8–2 eV for the outer-shell valence orbitals and 15–20 eV for the core ionization energies.

Appendix B. Total electron-impact cross sections of THF, TMP, PY and PU

Total electron-impact cross sections of THF, TMP, PY and PU, obtained from the evaluated model functions, are given in Tables 7 and 8 together with the evaluated uncertainties. Uncertainties of ionization cross sections were not determined for energies lower than 20–30 eV as no experimental data were available, on the one hand, and the BEB model may not be accurate at energies close to the ionization threshold, on the other hand. Subsequently, the uncertainties of excitation cross sections were also omitted in the respective energy region.

References

Alizadeh, E., Orlando, T.M., Sanche, L., 2015. Ann. Rev. Phys. Chem. 66, 379.
Allan, M., 2007. J. Phys. B 40, 3531.
Baek, W.Y., Bug, M.U., Rabus, H., 2014. Phys. Rev. A 89, 062716.
Baek, W.Y., Bug, M., Rabus, H., Gargioni, E., Grosswendt, B., 2012. Phys. Rev. A 86, 032702.
Baek, W.Y., Arndt, A., Bug, M.U., Rabus, H., Wang, M., 2013. Phys. Rev. A 88, 032702.
Baek, W.Y., 2016a. unpublished.
Baek, W.Y., 2016b. unpublished.
Baek, W.Y., Physikalisch-Technische Bundesanstalt, Braunschweig, Germany, private communication.
Bernhardt, P., Paretzke, H.G., 2003. Int. J. Mass Spectrom. 223–224, 599.
Blanco, F., García, G., 2009. J. Phys. B 42, 145203.
Bolorizadeh, M.A., Rudd, M.E., 1986. Phys. Rev. A 33, 882.
Bouchiha, D., Gorfinkiel, J.D., Caron, L.G., Sanche, L., 2006. J. Phys. B 39, 975.
Bransden, B.H., Joachain, C.J., 1983. Physics of Atoms and Molecules. Longman, London and New York, (ISBN 0-582-44401-2).
Bremner, L.J., Curtis, M.G., Walker, I.C., 1991. J. Chem. Soc. Faraday Trans. 87, 1049.
Bug, M.U., Hilgers, G., Baek, W.Y., Rabus, H., 2014. Eur. Phys. J. D. 68, 217.
Bug, M.U., 2014. Dissertation, University of Wollongong, Australia, URL ⟨http://ro.uow.edu.au/theses/4150/⟩.
Champion, C., 2013. J. Chem. Phys. 138, 184306.
Champion, C., 2014. Eur. Phys. J. D. 68, 205.
Champion, C., Quinto, M.A., Weck, P.F., 2015. Eur. Phys. J. D. 69, 127.
Chiari, L., Anderson, E., Tattersall, W., Machacek, J.R., Palihawadana, P., Makochekanwa, C., Sullivan, J.P., García, G., Blanco, F., McEachran, R.P., et al., 2013. J. Chem. Phys. 138, 074301.
Colyer, C.J., Vizcaino, V., Sullivan, J.P., Brunger, M.J., Buckman, S.J., 2007. New. J. Phys. 9, 41.
Dampc, M., Linert, I., Milosavljević, A.R., Zubek, M., 2007b. Chem. Phys. Lett. 443, 17.
Dampc, M., Szymańska, E., Mielewska, B., Zubek, M., 2011. J. Phys. B 44, 055206.

Dampc, M., Milosavljević, A.R., Linert, I., Marinković, B.P., Zubek, M., 2007a. Phys. Rev. A 75, 042710.
Do, T.P.T., Leung, M., Fuss, M., García, G., Blanco, F., Ratnavelu, K., Brunger, M.J., 2011. J. Chem. Phys. 134, 144302.
Do, T.P.T., Duque, H.V., Lopes, M.C.A., Konovalov, D.A., White, R.D., Brunger, M.J., Jones, D.B., 2015. J. Chem. Phys. 142, 124306.
Domaracka, A., Możejko, P., Ptasińska-Denga, E., Szmytkowski, C., 2007. Phys. Rev. A 76, 042701.
Domaracka, A., Możejko, P., Ptasińska-Denga, E., Szmytkowski, C., 2008. Publ. Astron. Obs. Belgrade 84, 35.
Duflot, D., Flament, J.-.P., Heinesch, J., Hubin-Franskin, M.-.J., 2010. Chem. Phys. Lett. 495, 27.
Edel, S., Terrissol, M., Peudon, A., Kümmerle, E., Pomplun, E., 2006. Radiat. Prot. Dosim. 122, 136.
Ferraz, J.R., dos Santos, A.S., de Souza, G.L.C., Zanelato, A.I., Alves, T.R.M., Lee, M.-.T., Brescansin, L.M., Lucchese, R.R., Machado, L.E., 2013. Phys. Rev. A 87, 032717.
Ferreira da Silva, F., Almeida, D., Martins, G., Milosavljević, A.R., Marinković, B.P., Hoffmann, S.V., Mason, N.J., Nunes, Y., García, G., Limão-Vieira, P., 2010. Phys. Chem. Chem. Phys. 12, 6717.
Fuss, M., Sanz, A.G., Blanco, F., Limão-Vieira, P., Brunger, M.J., García, G., 2014. Eur. Phys. J. D. 68, 161.
Fuss, M., Muñoz, A., Oller, J.C., Blanco, F., Almeida, D., Limão-Vieira, P., Do, T.P.D., Brunger, M.J., García, G., 2009. Phys. Rev. A 80, 052709.
Fuss, M.C., Sanz, A.G., Blanco, F., Oller, J.C., Limão-Vieira, P., Brunger, M.J., García, G., 2013. Phys. Rev. A 88, 042702.
Gauf, A., Hargreaves, L.R., Jo, A., Tanner, J., Khakoo, M.A., Walls, T., Winstead, C., McKoy, V., 2012. Phys. Rev. A 85, 052717.
Giuliani, A., Limão-Vieira, P., Duflot, D., Milosavljević, A.R., Marincović, B.P., Hoffmann, S.V., Mason, N., Delwiche, J., Hubin-Franskin, M.-.J., 2008. Eur. Phys. J. D. 51, 97.
Gordon research group, The General Atomic and Molecular Electronic Structure System (GAMESS), ⟨http://www.msg.ameslab.gov/gamess/⟩, online, accessed 10/2013.
Grosswendt, B., Waibel, E., 1978. Nucl. Instrum. Meth 155, 145.
Gupta, D., Naghma, R., Antony, B., 2014. Molec. Phys. 112, 1201.
Homem, M.G.P., Sugohara, R.T., Sanches, I.P., Lee, M.T., Iga, I., 2009. Phys. Rev. A 80, 032705.
Hush, N.S., Cheung, A.S., 1975. Chem. Phys. Lett. 34, 11.
Hwang, W., Kim, Y.-.K., Rudd, M.E., 1996. J. Chem. Phys. 104, 2956.
Incerti, S., Ivanchenko, A., Karamitros, M., Mantero, A., Moretto, P., Tran, H.N., Mascialino, B., Champion, C., Ivanchenko, V.N., Bernal, M.A., et al., 2010. Med. Phys. 37, 4692.
Inokuti, M., 1991. Radiat. Eff. Defects Solids 117, 143.
Irikura, K.K., Ali, M.A., Kim, Y.-.K., 2003. Int. J. Mass Spectrom. 222, 189.
Itikawa, Y., 2006. J. Phys. Chem. Ref. Data 35, 31.
Itikawa, Y., 2009. J. Phys. Chem. Ref. Data 38, 1.
Jones, D.B., Bellm, S.M., Blanco, F., Fuss, M., García, G., Limão-Vieira, P., Brunger, M.J., 2012. J. Chem. Phys. 137, 074304.
Khakoo, M.A., Orton, D., Hargreaves, L.R., Meyer, N., 2013. Phys. Rev. A 88, 012705.
Kim, Y.-.K., Rudd, M.E., 1994. Phys. Rev. A 50, 3954.
Kim, Y.-.K., Santos, J.P., Parente, F., 2000. Phys. Rev. A 62, 052710.
Limbachiya, C., Vinodkumar, M., Swadia, M., Joshipura, K.N., Mason, N., 2015. Molec. Phys. 113, 55.
Linert, I., Dampc, M., Mielewska, B., Zubek, M., 2012. Eur. Phys. J. D. 66, 20.
Llovet, X., Powell, C.J., Salvat, F., Jablonski, A., 2014. J. Phys. Chem. Ref. Data 43, 013102.
Maljković, J.B., Milosavljević, A.R., Blanco, F., Šević, D., García, G., Marinković, B.P., 2009. Phys. Rev. A 79, 052706.
Mašín, Z., Gorfinkiel, J.D., Jones, D.B., Bellm, S.M., Brunger, M.J., 2012. J. Chem. Phys. 136, 144310.
Milosavljević, A.R., Giuliani, A., Šević, D., Hubin-Franskin, M.-.J., Marinković, B.P., 2005. Eur. Phys. J. D. 35, 411.
Możejko, P., Sanche, L., 2003. Radiat. Environ. Biophys. 42, 201.
Możejko, P., Sanche, L., 2005. Radiat. Phys. Chem. 73, 77.
Możejko, P., Ptasińska-Denga, E., Domaracka, A., Szmytkowski, C., 2006. Phys. Rev. A 74, 012708.
National Institute of Standards and Technology (NIST), Computational chemistry comparison and benchmark database, ⟨⟩http://cccbdb.nist.gov/, online, accessed 10/2013.
Palihawadana, P., Sullivan, J.P., Buckman, S.J., Brunger, M.J., 2012. J. Chem. Phys. 137, 204307.
Palihawadana, P., Sullivan, J., Brunger, M., Winstead, C., McKoy, V., García, G., Blanco, F., Buckman, S., 2011. Phys. Rev. A 84, 062702.
Rudd, M.E., 1991. Phys. Rev. A 44, 1644.
Sanche, L., 2005. Eur. Phys. J. D. 35, 367.
Sanz, A.G., Fuss, M.C., Blanco, F., Mašin, Z., Gorfinkiel, J.D., Carelli, F., Sebastianelli, F., Gianturco, F.A., García, G., 2014. Appl. Radiat. Isot. 83, 57.
Shafranyosh, I.I., Sukjoviya, M.I., Shafranyosh, M.I., 2006. J. Phys. B 39, 4155.
Stener, M., Decleva, P., Holland, D.M.P., Shaw, D.A., 2011. J. Phys. B 44, 075203.
Sueoka, O., Mori, S., 1986. J. Phys. B 19, 4035.
Szmytkowski, C., 1989. Z. Phys. D. 13, 69.
T. International Commission on Radiation Units and Measurements (ICRU), 1996. Secondary electron spectra from charged particle interactions (ICRU report no. 55).
T. International Commission on Radiation Units and Measurements (ICRU), 2007. Elastic scattering of electrons and positrons (ICRU report no.77).
Tan, Z., Xia, Y., Liu, X., Zhao, M., Ji, Y., Huang, B., 2004. Radiat. Environ. Biophys. 43, 173.
Tanaka, H., Okada, T., Boesten, L., Suzuki, T., Yamamoto, T., Kubo, M., 1982. J. Phys. B 15, 3305.
Tasaki, K., Yang, X., Urano, S., Fetzer, S., LeBreton, P.R., 1990. J. Am. Chem. Soc. 112, 538.
Trevisan, C.S., Orel, A.E., Rescigno, T.N., 2006. J. Phys. B 39, L255.
Uehara, S., Nikjoo, H., Goodhead, D.T., 1992. Phys. Med. Biol. 37, 1841.
Winstead, C., McKoy, V., 2006. J. Chem. Phys. 125, 074302.
Wolff, W., Luna, H., Sigaud, L., Tavares, A.C., Montenegro, E.C., 2014. J. Chem. Phys. 140, 064309.
Yoon, J.-.S., Song, M.-.Y., Han, J.-.M., Hwang, S.H., Chang, W.-.S., Lee, B.J., Itikawa, Y., 2008. J. Phys. Chem. Ref. Data 37, 913.
Zecca, A., Perazzolli, C., Brunger, M.J., 2005. J. Phys. B 38, 2079.
Zecca, A., Chiari, L., García, G., Blanco, F., Trainotti, E., Brunger, M.J., 2010. J. Phys. B 43, 215204.